LAS-TR-207-5
March 1962

AFOSR-2432
AF 49 (638) 1033

EXPERIMENTAL INVESTIGATIONS OF TRANSPORT PROPERTIES OF PARTIALLY IONIZED GASES

P. J. Dickerman

FINAL REPORT

Prepared for

Air Force Office of Scientific Research
Office of Aerospace Research

Contract No. AF 49(638)-1033
Project No. 9781, Task No. 37713

THE UNIVERSITY OF CHICAGO
LABORATORIES FOR APPLIED SCIENCES
CHICAGO 37, ILLINOIS

NOTICES

When Government drawings, specifications, or other data are used for any purpose other than in connection with a definitely related Government procurement operation, the United States Government thereby incurs no responsibility nor any obligation whatsoever; and the fact that the Government may have formulated, furnished, or in any way supplied the said drawings, specifications, or other data, is not to be regarded by implication or otherwise as in any manner licensing the holder or any other person or corporation, or conveying any rights or permission to manufacture, use, or sell any patented invention that may in any way be related thereto.

Qualified requesters may obtain copies of this report from the Armed Services Technical Information Agency, (ASTIA), Arlington Hall Station, Arlington 12, Virginia.

This report has been released to the Office of Technical Services, U. S. Department of Commerce, Washington 25, D. C., for sale to the general public.

FOREWORD

This is the first annual report, covering the period 15 February 1961 to 15 February 1962, on LAS Task 207, "Research on Experimental Investigations of Transport Properties of Partially Ionized Gases." This program is conducted by the Laboratories for Applied Sciences (LAS) of the University of Chicago for the Air Force Office of Scientific Research under Contract No. AF 49(638)-1035.

University of Chicago personnel who participated in the work covered by this report include: B. P. Alpiner, R. W. Deuel, P. J. Dickerman, H. Halle, and J. R. Hoenig.

ABSTRACT

Recent advances in electric arc research and development allow stable high-temperature environments to be obtained over extended periods of time in the laboratory. By making use of the known relationships between temperature and conductivity in such arc discharges and by experimentally measuring the current density, electron density, and temperature, the effective cross section of atoms which impede the electron flow can be determined. Thus, atom-electron collision cross sections can now be measured in the interesting energy range of 1 to 2 ev, lower than heretofore possible using conventional beam apparatus. Techniques involved in making the necessary spectroscopic and electrical measurements are given, and results obtained for three gases (argon, helium, and nitrogen) are presented. These results are then used to determine several of the transport properties for these partially ionized gases.

TABLE OF CONTENTS

LIST OF ILLUSTRATIONS

LIST OF ILLUSTRATIONS (cont'd)

LIST OF TABLES

1. INTRODUCTION

In considering the rates of certain physical processes and in order to understand many of the important aspects of hydrodynamics, magnetohydrodynamics, and plasma physics, it is necessary to discuss the transport of matter, energy, momentum, and electrical charge by atomic systems. The transport of matter is described by various diffusion coefficients, the transport of energy by the thermal conductivity, the transport of momentum by the viscosity, and the transport of electrical charge by the electrical conductivity. These four quantities (diffusion coefficients, thermal conductivity, viscosity, and electrical conductivity) are thus known as the transport properties.

The fundamental atomic parameters upon which these transport properties depend are the collision cross sections. These cross sections, of course, depend upon particle velocity, or macroscopically speaking, upon the gas temperature. Therefore, measurements must be performed on a system which is precisely within the energy range of interest. Since this work was motivated by the need for data at energies below 2 ev (re-entry conditions, certain astrophysical conditions, shock and detonation wave energies), a new experimental technique using a stable electric arc discharge was employed. It should be noted here that cross-section measurements have been made for many elements in the past using one or another of several beam techniques. However, all of these methods become insensitive below a few volts, necessitating a different experimental approach for the above-mentioned energy range.

It was not the purpose of the present work to generally develop arc technology and experimental techniques, although to be sure several new procedures were found in the course of the program, but rather to

make use of existing knowledge and apply it to the problem of measuring cross sections. The principal difference between the arc and beam methods is that measurements of an arc discharge provide an "effective" cross section (velocities averaged over some distribution), whereas a beam technique yields data for a unique collision velocity. A considerable amount of work [1, 2, 3]*, however, has shown that local thermodynamic equilibrium (LTE) prevails for arcs run at atmospheric pressure and at temperatures less than 10 ev, since for this condition excitation and de-excitation and ionization and recombination are mainly caused by electron collisions. Thus one is assured that the velocity distribution is maxwellian and that the data obtained here are sufficiently general to be safely applied to other systems with appropriate energies and densities.

2. DISCUSSION

2.1 PREVIOUS WORK

The problem of determining cross sections for atom-electron collisions is one that had received considerable attention in the past but, like many atomic physics activities, has not been pursued actively in recent years. The work probably had its start with the measurement of the absorption coefficient for slow electrons in gases by Lenard [4] and later by Ramsauer [5] and Mayer [6]. The method used by Ramsauer and several succeeding workers made use of a series of slits arranged in a circle with the electron paths being bent into this circle by a magnetic field. A measure of the emission current of the filament (electron beam source) and the current collected at the end of the path yielded the total

* Numbers in brackets refer to entries in the Bibliography.

attenuation and hence a total collision probability. Data were obtained for a number of elements, and relatively good agreement between individual workers may be found in the energy range of about 4 to 100 ev. Total collision cross sections with electrons are available for such things as H_2, He, A, Ne, N_2, CO, CO_2, Xe, and Kr. However, note that only molecular cross sections are available for diatomic elements. Further, a rather general state of experimental disagreement exists at lower energies, which are of interest from the standpoint of plasma physics. Figure 1, taken from Brown's book [7] on plasma physics, is an example of data at this lower energy range. Practically no data for other elements is available. This program therefore has as its purpose the determination of atom-electron collision cross sections using the new arc technique for the energy range of Figure 1 and for a selection of elements of present-day interest.

2.2 CROSS-SECTION DETERMINATIONS USING THE ELECTRIC ARC

Experimental work can be performed using a stable, cylindrically symmetric arc operating at approximately 1 atmosphere of pressure. The element of interest can in principle be introduced either as the ambient gas or by a controlled process of electrode erosion.

Now the relation between electrical conductivity, the current density, and the electric field strength is given by Ohm's law as

$$\sigma = \frac{J}{E} \quad . \tag{1}$$

The electrical conductivity σ can be measured directly, and it is also possible to obtain the temperature distribution in an arc by spectroscopic

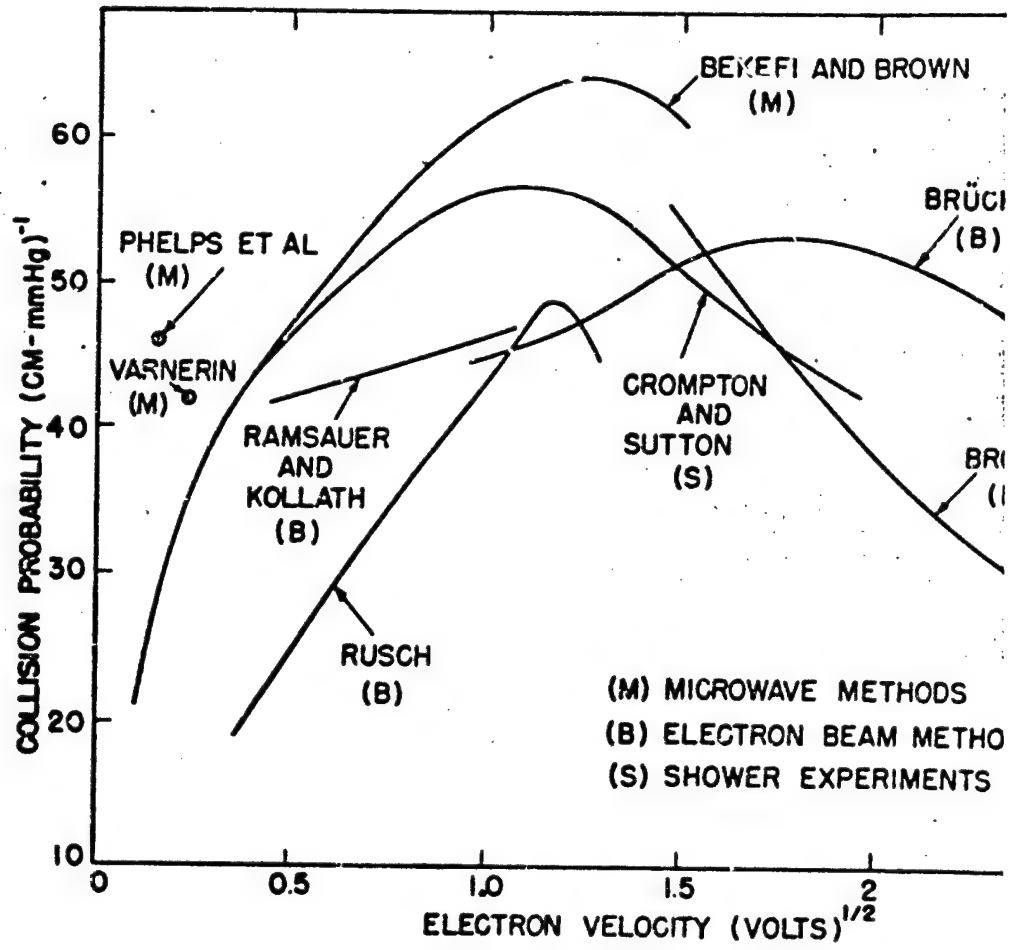

Figure 1. Low-Energy Collision Probabilities in Hydr

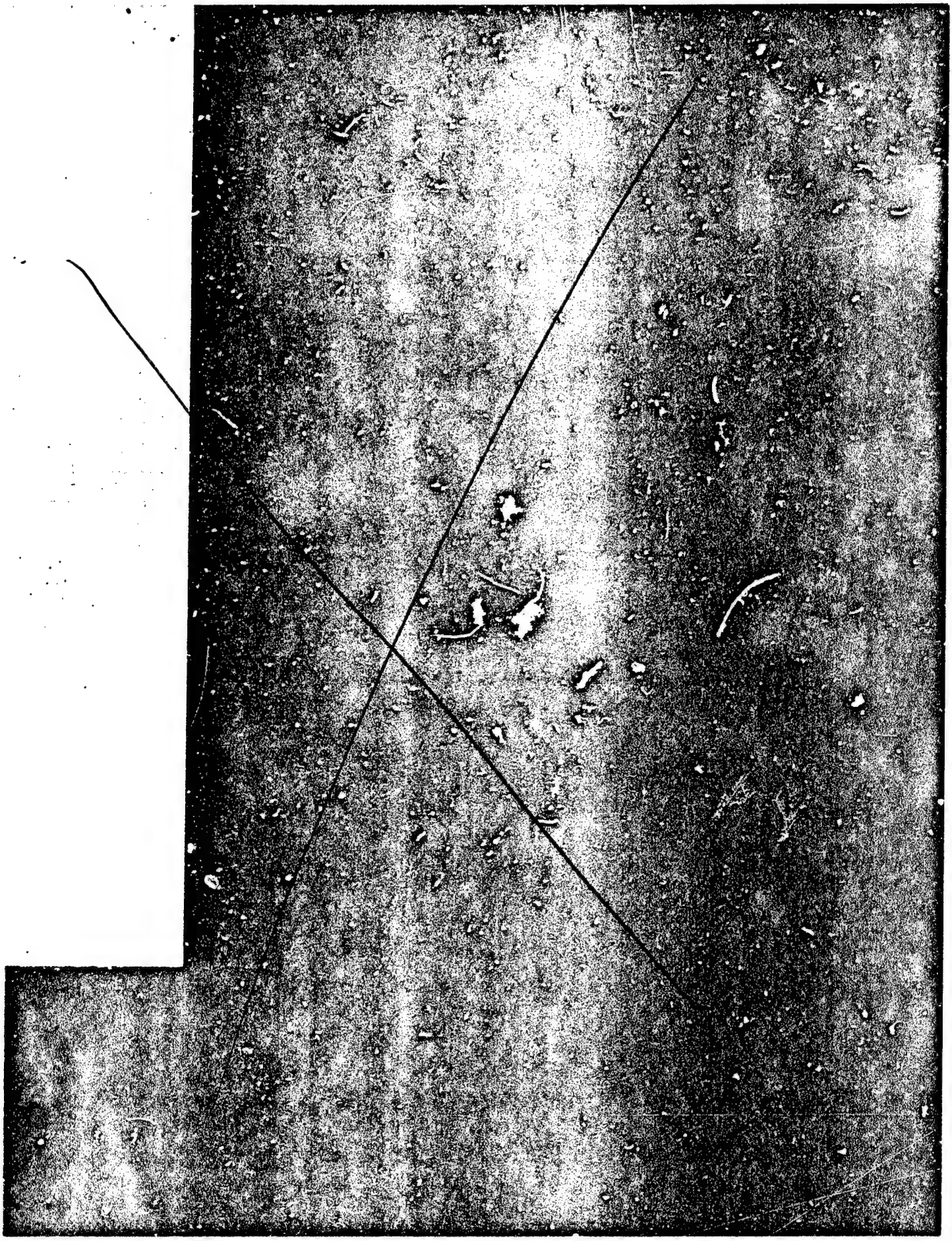

techniques. Therefore, a relation between temperature and conductivity must be obtained using the concept of charge transport by electrons in the arc plasma. In obtaining this relation, one can neglect the contribution of the ions because of their much lower mobility.

In the simplest case, if v_e is the mean thermal velocity of electrons, λ_e the mean free path, and τ_e the mean interval between collisions,

$$\tau_e = \frac{\lambda_e}{v_e} \quad . \tag{2}$$

If the electron is in the presence of an electric field, then during the time τ_e the electron falls freely in the electric field a distance

$$D = \frac{eE}{2m_e} \tau_e^2 \quad , \tag{3}$$

where e is the electronic charge and m_e the mass of the electron. Thus the average velocity (drift velocity) in the direction of the electric field is

$$u_e = \frac{D}{\tau} = \frac{e\lambda_e}{2m_e v_e} E \quad . \tag{4}$$

This gives the electron mobility, in terms of the mean free path and thermal velocity, as

$$b_e = \frac{e\lambda_e}{m_e v_e} \quad . \tag{5}$$

It should be realized that in the general case the mobility is a function of the electric field strength. However, a simple calculation shows that for the conditions of the experiment, Eq. (5) is a good approximation. As long as the electron temperature T_e is approximately equal to the heavy particle temperature (gas temperature) T_M, the drift is proportional to the electric field as given above. Now the electronic temperature becomes considerably different from the gas temperature when $\lambda_e E$ increases beyond the value given by

$$\lambda_e E = \frac{1}{\epsilon} \sqrt{\frac{m_e}{M}} \, T_M , \qquad (6)$$

where ϵ is the conversion factor between electron volts and temperature. The R. H. S. of Eq. (6) is ≥ 0.03 for the energy range of interest. Further, λ_e can be taken as approximately 10^{-3} cm for the condition at which our arc operates (atmospheric pressure and greater than $10^{4}\,^{o}$K). Thus the electric field should generally be ≤ 30 volts/cm for our approximation to be valid and for complete equilibrium to be maintained. All data presented in this report correspond to field strengths well below this critical value.

Once again now, using Ohm's law, one finds that the electrical conductivity can be expressed as

$$\sigma = \frac{e^2 n_e \lambda_e}{m_e v_e} . \qquad (7)$$

If one now introduces the gas-kinetic relation for the thermal velocity and expresses the mean free path in terms of the collision cross sections Q, the conductivity is related to the temperature, electron and atom

concentrations, and cross sections of atoms and ions against electrons by the expression

$$\sigma = \frac{J}{E} = \frac{e^2 n_e}{\left(\frac{8mKT}{\pi}\right)^{1/2}} \cdot \frac{1}{n_a Q_e^{\,a} + n_i Q_e^{\,i}} \quad . \qquad (8)$$

In general, the symbol $Q_j^{\,k}$ is used in this report to denote the total effective collision cross section for particles of kind j against particles of kind k. Note that if necessary the term $n_a Q_e^{\,a}$ can be divided in the presence of several atom species into $n_1 Q_1 + n_2 Q_2 + \cdots$ and the term $n_i Q_e^{\,i}$ into $n_+ Q_+ + n_{++} Q_{++} + \cdots$ in the presence of ions of multiple charge.

At this point it becomes necessary to discuss the geometry of the particular arc used in the experiments. Figure 2 shows this arc chamber along with electrode shapes and cooling water flow channels. Normally all parameters associated with an arc are functions of the column radius, so that spatially resolved measurements are required. However, Olsen [8] has shown that for the geometry used here the electric field is not a function of radius in the vicinity of the flat anode. Thus a single measurement of the field strength determines its value for all arc radii in this region. The current density, on the other hand, is a strong function of radius. The same is true for the temperature and number densities, which are related by the Saha equation and are measured spectroscopically. Measurements of these latter parameters then along with the field strength, in conjunction with the use of Eq. (8), provide the means for determining the cross sections as functions of the arc radius or plasma temperature. The temperature range that one can conveniently cover by this method lies approximately between 1 and 2 ev, with extensions possible under certain conditions.

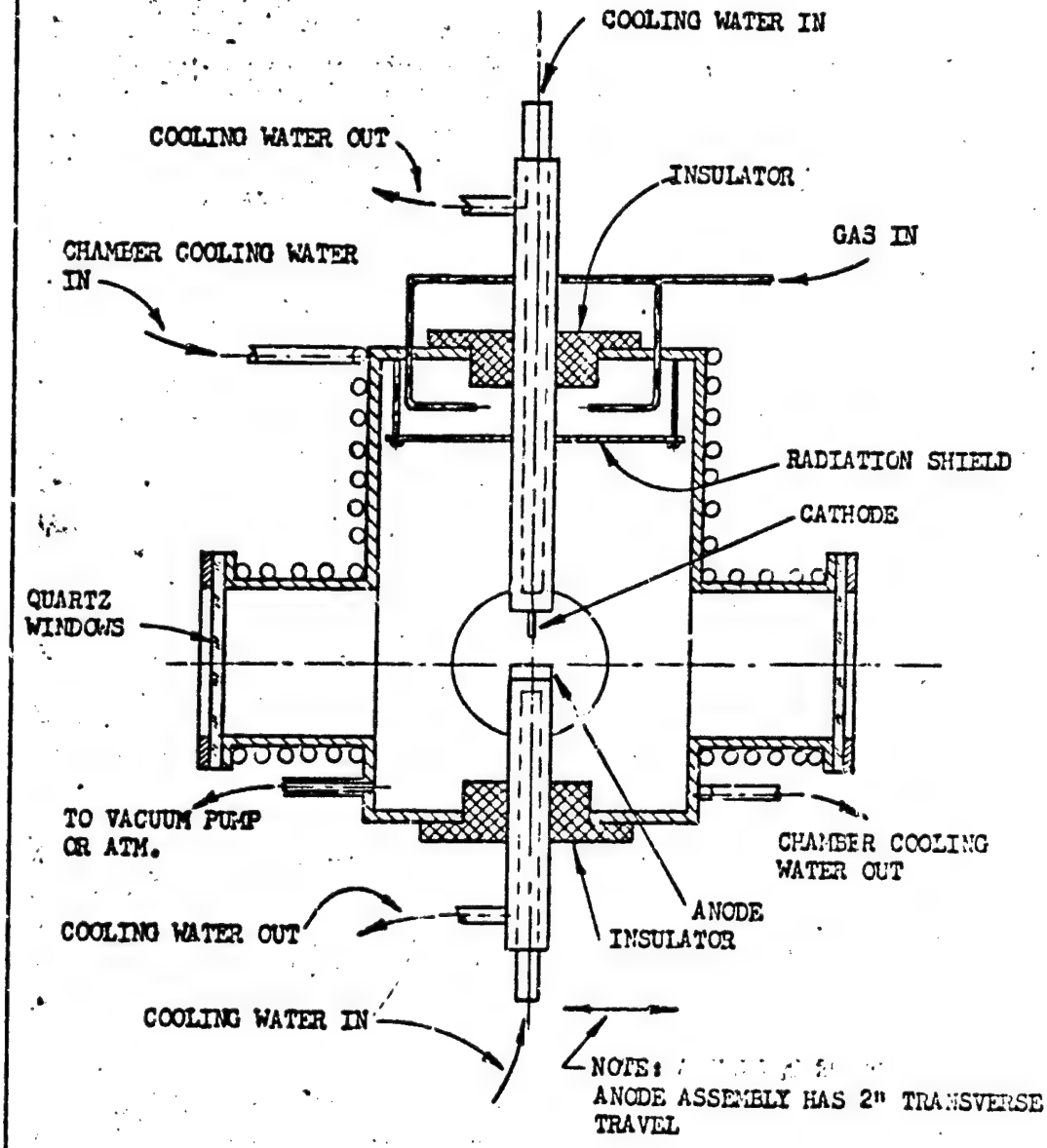

FIG. 2 SCHEMATIC DIAGRAM OF THE EXPERIMENTAL ARC CHAMBER

2.3 EXPERIMENTAL PREPARATIONS

At the outset of the program, this laboratory had had considerable experience in the development and operation of various arc plasma generators working at atmospheric pressure and with "vacuum arcs" operating at low pressures ($\approx 10^{-6}$ mm Hg) and in strong magnetic fields. It was originally planned to modify one of these arcs for use in making the cross-section measurements. However, work on these arcs immediately prior to starting this program showed extreme turbulence and instabilities in the case of the atmospheric pressure arcs and a lack of thermodynamic equilibrium for the vacuum arcs. It was necessary, therefore, as a first step in this research, to design and construct an arc which could operate at about one atmosphere of pressure, be free of any major instabilities, and also be free of contamination due to electrode erosion. The design finally chosen as being most favorable is similar to one used by Olsen [8] in making transition probability measurements. It is relative simple (see Figure 2) and had been shown to be extremely stable in operating characteristics.

The electrical power for the arc is provided by a set of three motor-generator sets, with several series or parallel combinations available. A maximum of 365 volts is available at 200 amps, or a maximum current of 900 amps can be obtained at 120 volts. A ballast resistor, constructed in our shop, is used in series with the arc to provide the customary "drooping" volt-ampere characteristics for the power supply.

When first put into use, it was necessary to qualitatively assess the arc operation and to investigate briefly such parameters as electrical power, cathode size, arc length, and gas flow rates and their effects on arc stability.

Experiments quickly showed the importance of cathode size. In order to cover a range of currents from, say, 50 amps to 400 amps, it is necessary to use cathode sizes ranging from 0.060 inch to 0.120 inch in diameter. It was found that at the lower currents the cathodes larger than that necessary to supply the needed emission led to arc wandering and general instability, and, of course, at the higher currents the smaller cathodes suffered from erosion. Thus it is not possible to use any one cathode to cover the entire current range of interest.

The cathode material used has been 2 per cent thoriated tungsten in all cases. The anode material has been either copper, molybdenum, or tungsten, depending on the type of gas used for the experiment. During the first half of the program, it became clear that within the scope of this first year's effort probably three gases could be investigated. The three that were chosen, and for which the necessary computations were started, were argon, helium, and nitrogen. All these gases used for the experiment were certified to have less than 10 ppm of any impurity and were at least 99.997 per cent pure over-all. Argon and helium worked well with any anode, as may well have been expected. However, it was found to be impossible to operate a pure nitrogen arc without considerable erosion of any anode surface. Since erosion leads to contamination of the arc plasma by atoms of the electrode, this condition could hardly be tolerated. A solution was found by using a mixture of argon and nitrogen. As long as argon is present at 50 per cent partial pressure or greater, the copper anode can be used with negligible erosion. Continuous four-hour operation with no change in arc parameters indicates that a steady plasma free of contamination is obtained.

The precise ratio of gases to be used in this case was measured in the following way: Using the settings of regulator valves on argon and nitrogen gas cylinders which correspond to desired arc operation, the flow rates of argon and nitrogen were independently measured. A manometer was used to insure that individual pressures did not exceed atmospheric pressure by more than 1/2 cm Hg and did not differ from each other by more than 1/4 cm Hg.

When the gases passed from the high-pressure cylinder into the line leading to the chamber, they were cooled because of expansion. A large length of this line was used to warm the gas. The difference in temperature between the two gases was measured at the entrance of the flowmeter with a thermocouple. Knowing the pressure, temperature, and atomic weights of the two gases, their true flow rates were determined. This yielded the ratio, by volume, of argon to nitrogen. Since this ratio is kept constant during a running of the arc, a simple application of Dalton's law yields the particle number densities for each gas.

All experimental indications are that this arc besides being free of electrode contamination, is extremely stable in operation. High-speed motion pictures (4000 frames/sec) have indicated neither any visible fluctuations in arc intensity with time nor any spatial inhomogeneity. Photoelectric measurements of the total intensity of the arc have not revealed any fluctuations up to frequencies of 10 megacycles/sec, the limit of the measurements. Oscilloscope traces of arc voltage show a fluctuation of less than 1 per cent at a kilocycle and a megacycle, with all other perturbations being negligible. Thus it appears that the arc,

operating at atmospheric pressure, provides a steady-state, uncontaminated plasma with local thermodynamic equilibrium well established. Typical operation, shown for the case of argon at 50 amps and an arc length of 1/2 inch, is seen in Figure 3. Figure 4 is a photograph of the arc chamber and associated equipment, showing the 3.4-meter Ebert spectrograph in the background. Figure 5 shows the flat voltage-current characteristic for the gases and power ranges used for the experiments. The voltage rises sharply, of course, when the current approaches zero for all three cases.

2.4 PRELIMINARY CALCULATIONS

A number of computations were necessary so that experimental results could be used to deduce values for collision cross sections. In all cases, the work was done using a desk calculator. Although the establishment of a numerical program may have been justified for obtaining number densities, partition functions, etc., it was felt this procedure would not prove economical within the scope of the program.

For all of this work and for the spectroscopy that follows, we assume that LTE prevails, that is, that the kinetic temperatures of electrons, atoms, and ions and also the temperatures characterizing the distributions over bound states (Boltzmann factors) and free states (Saha equations) are alike. This assumption is justified by the facts that, for our range of temperatures and pressures, excitation and de-excitation by electron collisions are predominant and that our voltages in the arc column are less than the critical potentials (see Eq. 6 and Figure 5).

The partition functions and number densities for argon were taken directly from values tabulated by Olsen [8]. The particle densities

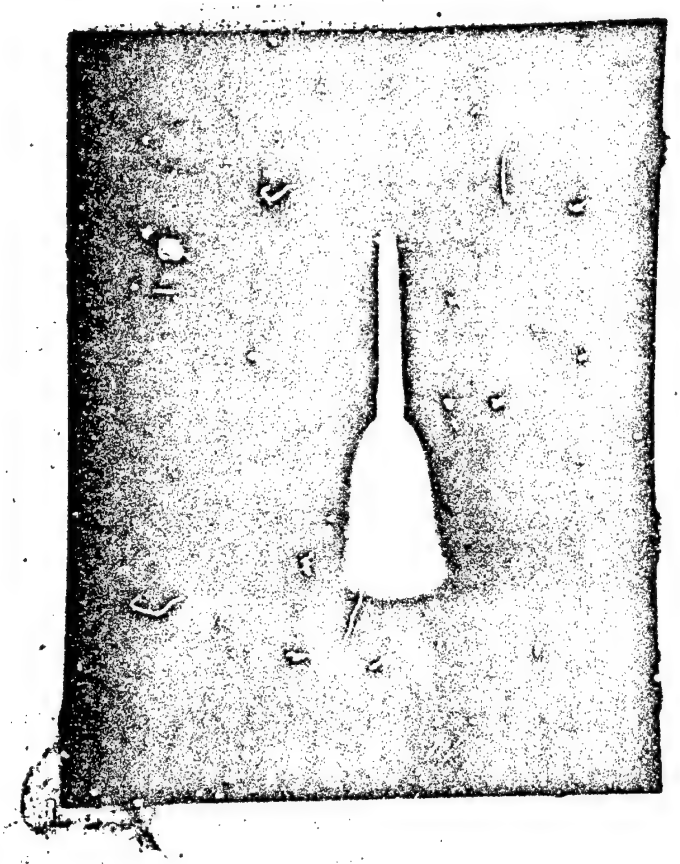

FIG. 3 PHOTOGRAPH OF ARC OPERATING AT 50 AMPS IN ARGON AT A LENGTH OF 1/2 INCH.

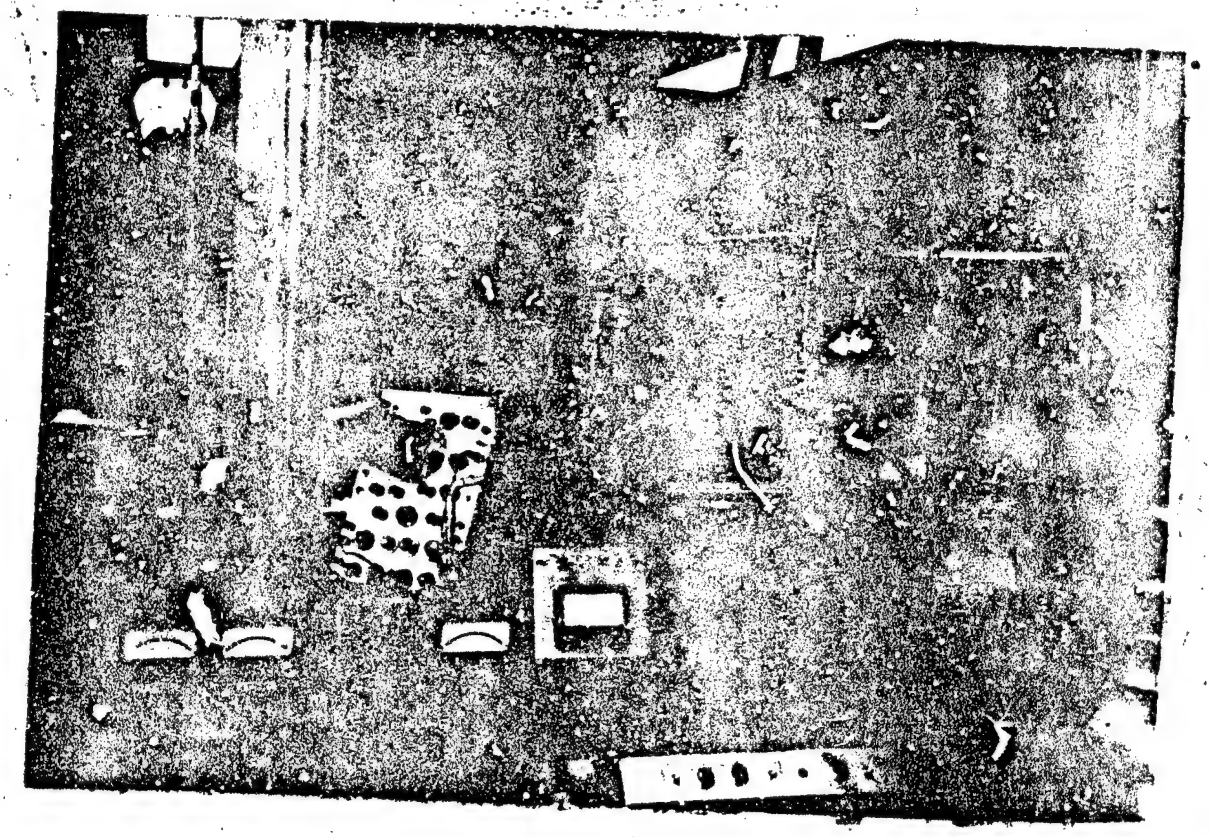

FIG. 4 PHOTOGRAPH OF ARC CHAMBER AND ASSOCIATED EQUIPMENT

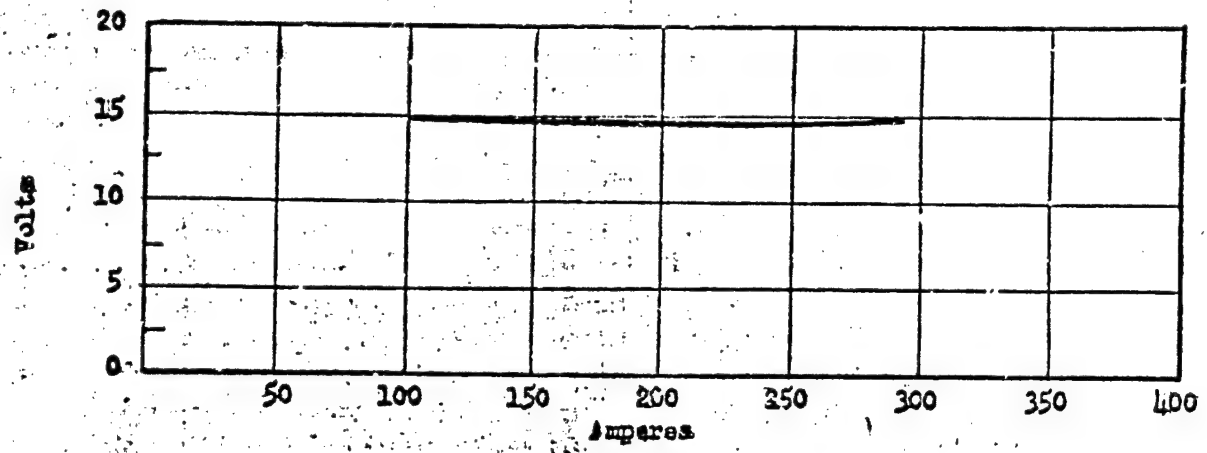

5 (a)

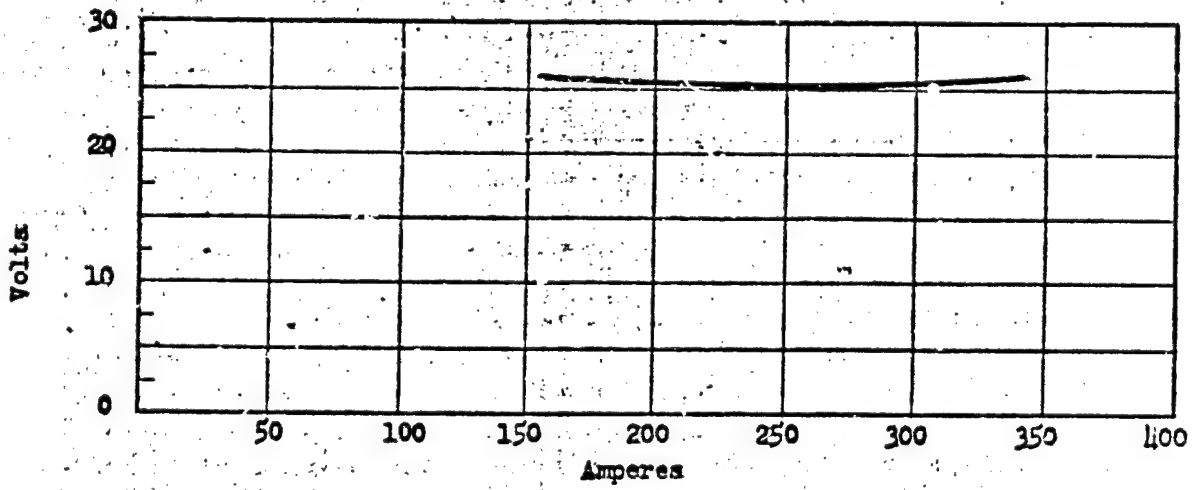

5 (b)

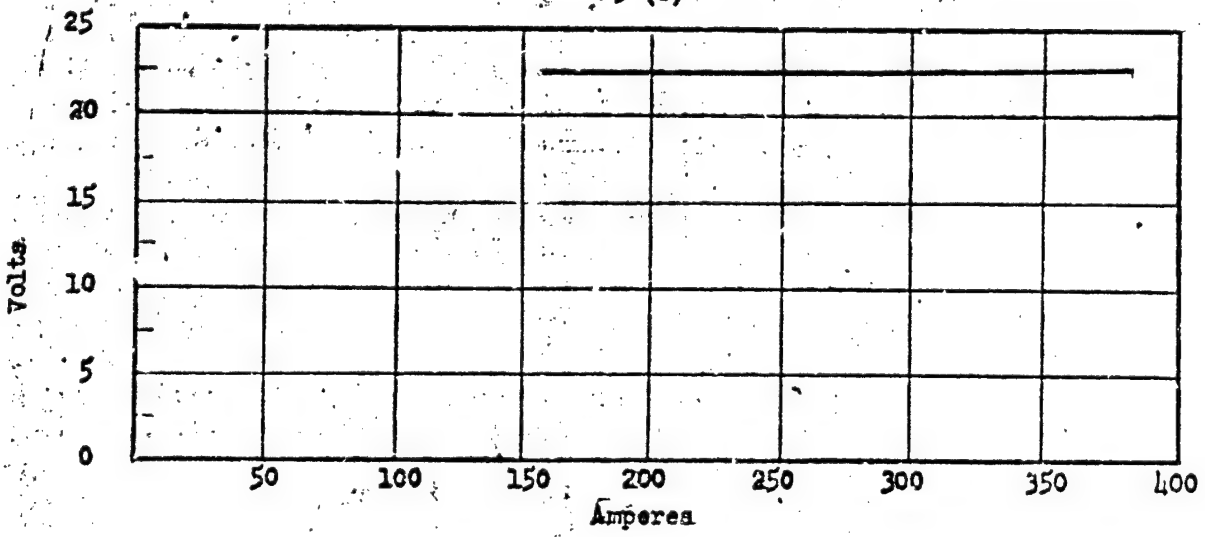

5 (c)

FIG. 5 VOLTAGE-CURRENT CHARACTERISTICS FOR 3/8" ARC USING: a) ARGON; b) HELIUM; AND c) 66% ARGON, 34% NITROGEN.

for the temperature range of interest are given in Figure 6, where n_o is the number density of atoms, n_+ of singly charged ions, n_e of electrons, and N the total particle density. In all cases the presence of doubly charged ions were tabulated. However, since their density is relatively small at these temperatures, they were omitted from the figures for the sake of convenience. The partition functions for helium were obtained from data presented by Barr, Cason, and Smith [9, 10]. Using this information, one can solve a set of equations (Saha relation, charge neutrality, Dalton's law) and obtain the particle densities in helium as a function of temperature. These data are given in Figure 7 for the case of atmospheric pressure.

The number densities for a pure nitrogen gas at atmospheric pressure had been tabulated by Burhorn and Wienecke [11] (see Figure 8), and it was at first anticipated that these data could be applied directly to a nitrogen arc. However, subsequent arc operation showed that severe electrode erosion always occurred in a pure nitrogen atmosphere. Data was therefore needed for a mixture of 34 per cent nitrogen, 66 per cent argon, which proved to operate satisfactorily. This was obtained by using the partition functions for nitrogen calculated by Cason and Smith [10], the partition functions for argon mentioned above, and solving a set of equations which were similar to, though more complicated than, those for the case of helium mentioned above.

The next step in the series of calculations is to make use of these number densities in calculating the ion-electron collision cross sections. At the outset of this program, it was not certain whether theoretical or experimental values should be obtained for these cross sections (these values are needed for the final calculations when obtaining atom-electron cross sections). A literature survey along with an estimate of these further experimental costs strongly favored the analytical method.

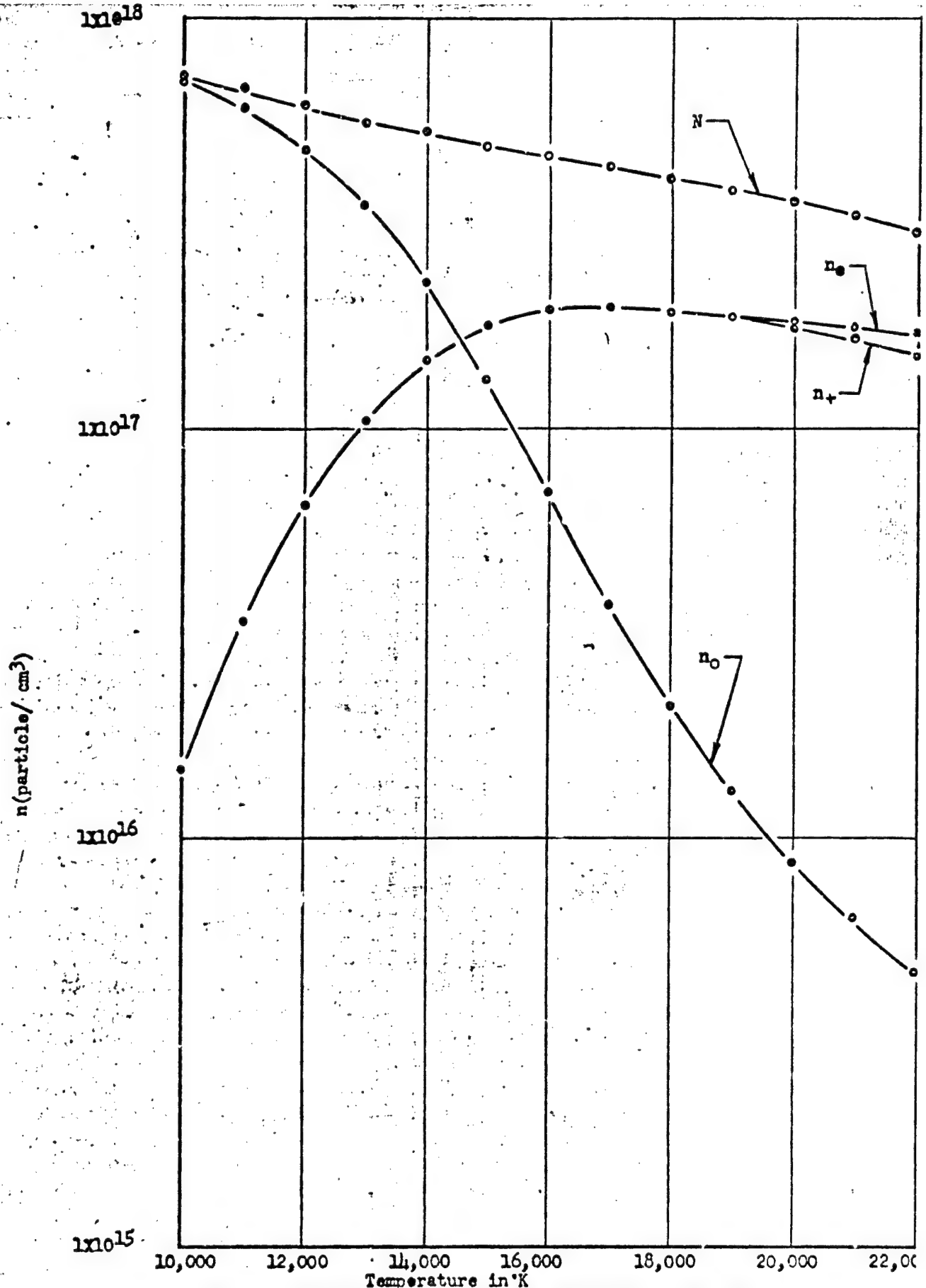

FIG. 6 PARTICLE DENSITIES FOR AN ATMOSPHERIC PRESSURE ARGON PLASMA

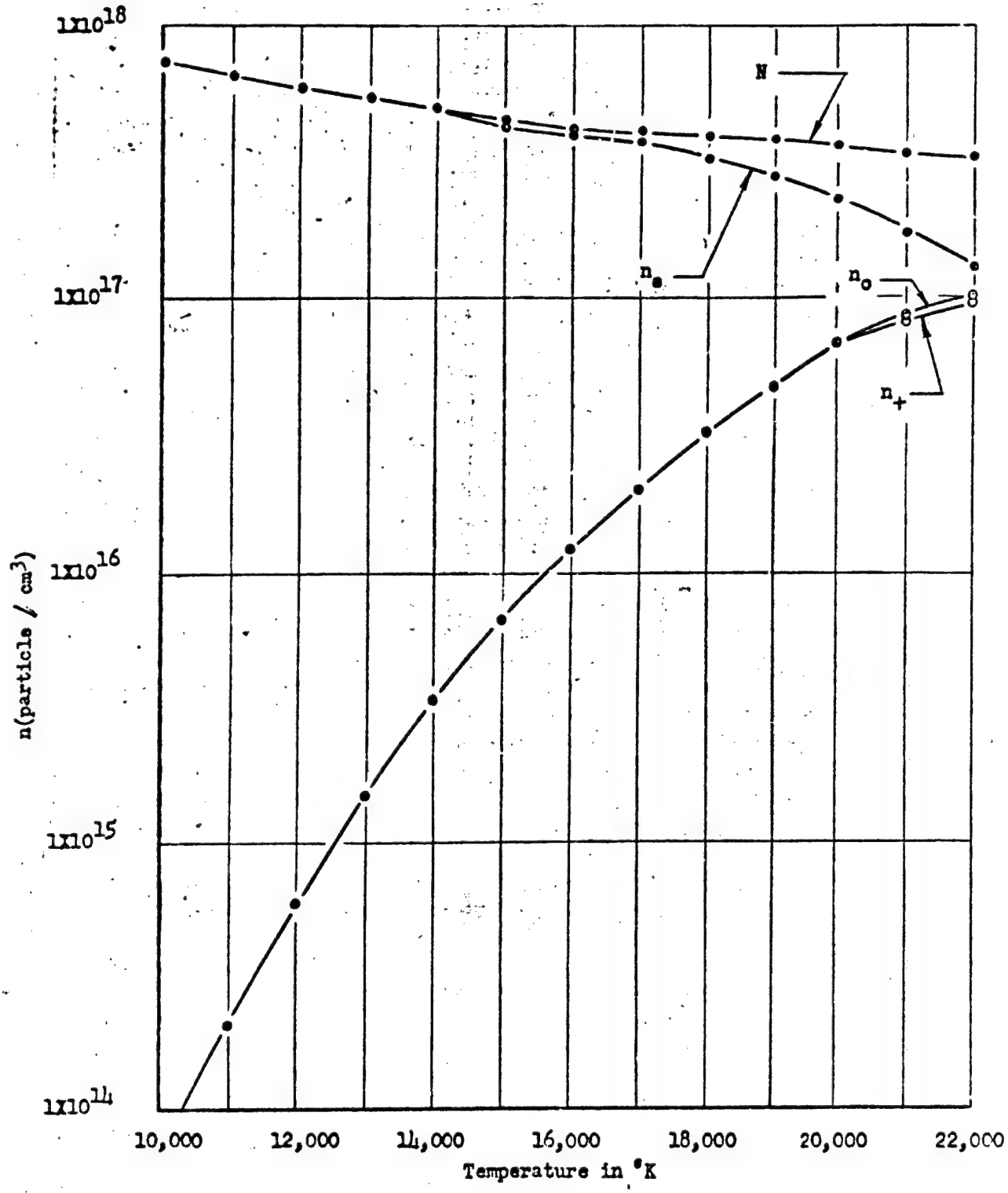

FIG. 7 PARTICLE DENSITIES FOR AN ATMOSPHERIC PRESSURE HELIUM PLASMA

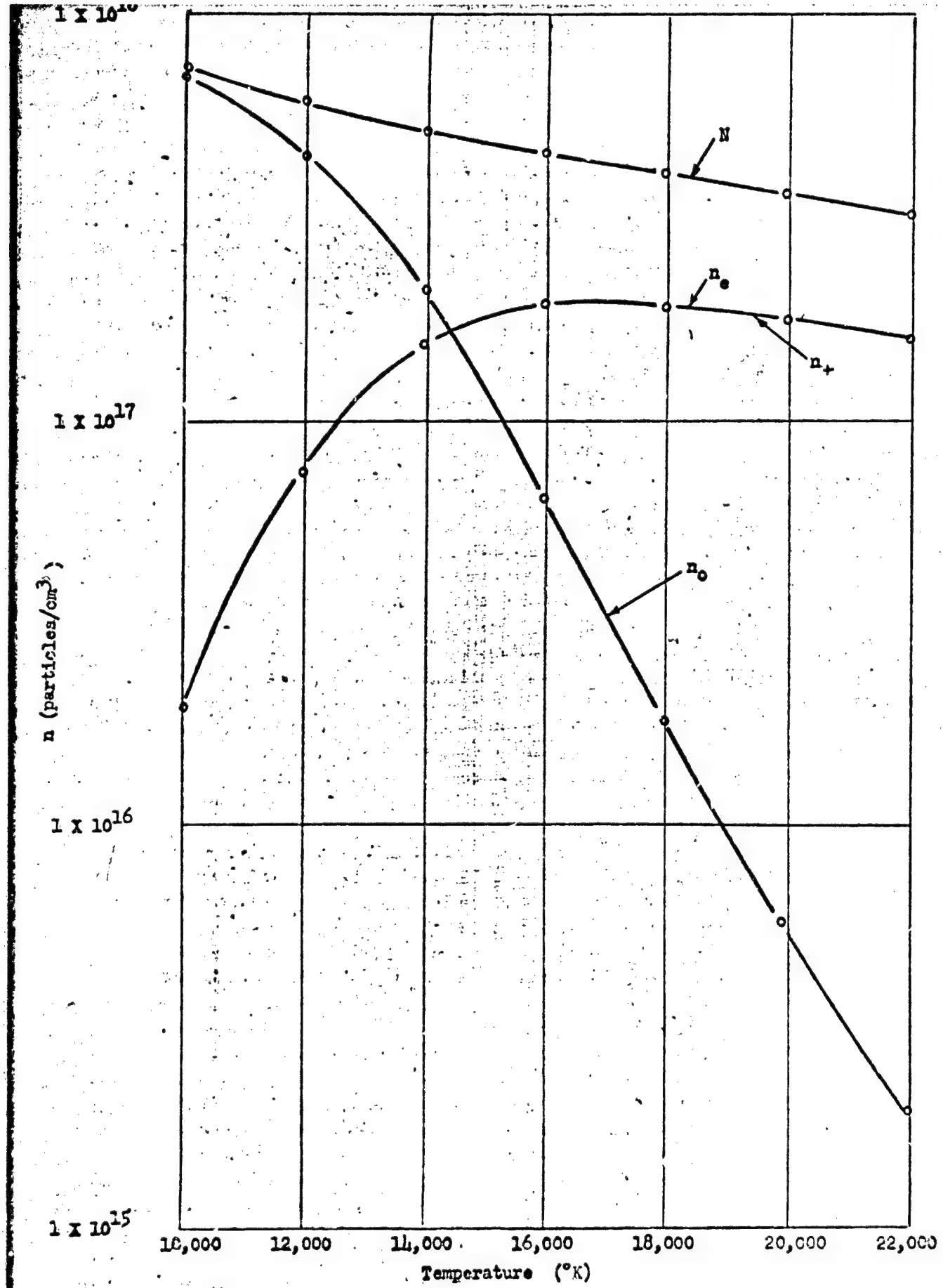

FIG. 8 PARTICLE DENSITIES FOR AN ATMOSPHERIC PRESSURE NITROGEN PLASMA

Now in order to obtain a relation for the ion-electron cross section, we can make use of Eq. (7) and rewrite it in the form

$$\sigma = \frac{e^2 n_e \lambda_e}{(3 m KT)^{1/2}} \quad . \tag{9}$$

According to Spitzer and Härm [12, 13], the electrical conductivity of a completely ionized gas is given by

$$\sigma = \frac{2 (KT)^{3/2} \gamma_E}{\left[\left(\frac{\pi}{2}\right)^{3/2} \left(m_e\right)^{1/2} e^2 Z \ln q\right]} \quad , \tag{10}$$

where

$$Z = \sum_i \frac{n_i Z_i^2}{n_e} \quad , \qquad q = \frac{KT}{e^2 Z n_+^{1/3}} \quad ,$$

n_+ is the number of ions/cm^3 having an effective charge Z per ion, and γ_E is a coefficient tabulated by Spitzer. This expression can be equated to the gas-kinetic expression (Eq. 9) for the case where λ_e contains no dependence on atoms and the ion-electron cross sections (Q_e^i) thereby obtained. This treatment by Spitzer apparently considers the mutual effect of electrons upon one another as contrasted with Gvosdovers theory, which will be mentioned below. The greatest uncertainty in Eq. (10) exists in the numerical value of the ($\ln$) term. Equating Eqs. (9) and (10) gives the following expression:

$$\sum_i n_i Q_i^e = \left[\frac{\left(\frac{\pi}{2}\right)^{3/2} \left(\frac{1}{3}\right)^{1/2}}{2}\right] \frac{e^4 n_e Z \ln q}{(KT)^2 \gamma_E} \quad . \tag{11}$$

Since we are interested in the temperature range below some 20,000°K, a simplification can be made. That is, that singly charged ions are the predominant ion species present. The R. H. S. of Eq. (11) is then simply $n_i Q_i^e$. Further, cancelling the n_i and n_e, the expression finally becomes

$$Q_i^e \approx (.4) \frac{\pi}{2} \frac{e^4}{(KT)^2} Z \frac{\ln g}{\gamma_E} \quad . \tag{12}$$

This is about half the value obtained by Gvosdover and Peters [14, 15] and is in good agreement with the preliminary results obtained in [18]. For $Z = 1$ and $\gamma_E = 0.5816$, one obtains within the accuracy of the measurements ($\approx \pm 10\%$) the simple expression

$$Q_i^e = \frac{e^4}{(KT)^2} \ln \left(\frac{KT}{e^2 n_i^{1/3}} \right) \quad . \tag{13}$$

Using the Rutherford scattering formula as applied to ions with charge Z, this can be converted to

$$Q_{Z+} = Z^2 Q_+ \quad . \tag{14}$$

Calculations based on these relations were made for the three gases, argon, helium, and nitrogen, for the appropriate temperature ranges. The results are shown in Figures 9, 10, and 11. Experimentally, of course, nitrogen was mixed with argon in a known ratio so as to prevent erosion. Therefore, in all calculations for this argon-nitrogen mixture, the nitrogen cross section data were combined with that for argon so that the terms $n_a Q_e^a$ and $n_i Q_e^i$ in Eq. (8) were actually sums over all the species present at their relative concentrations.

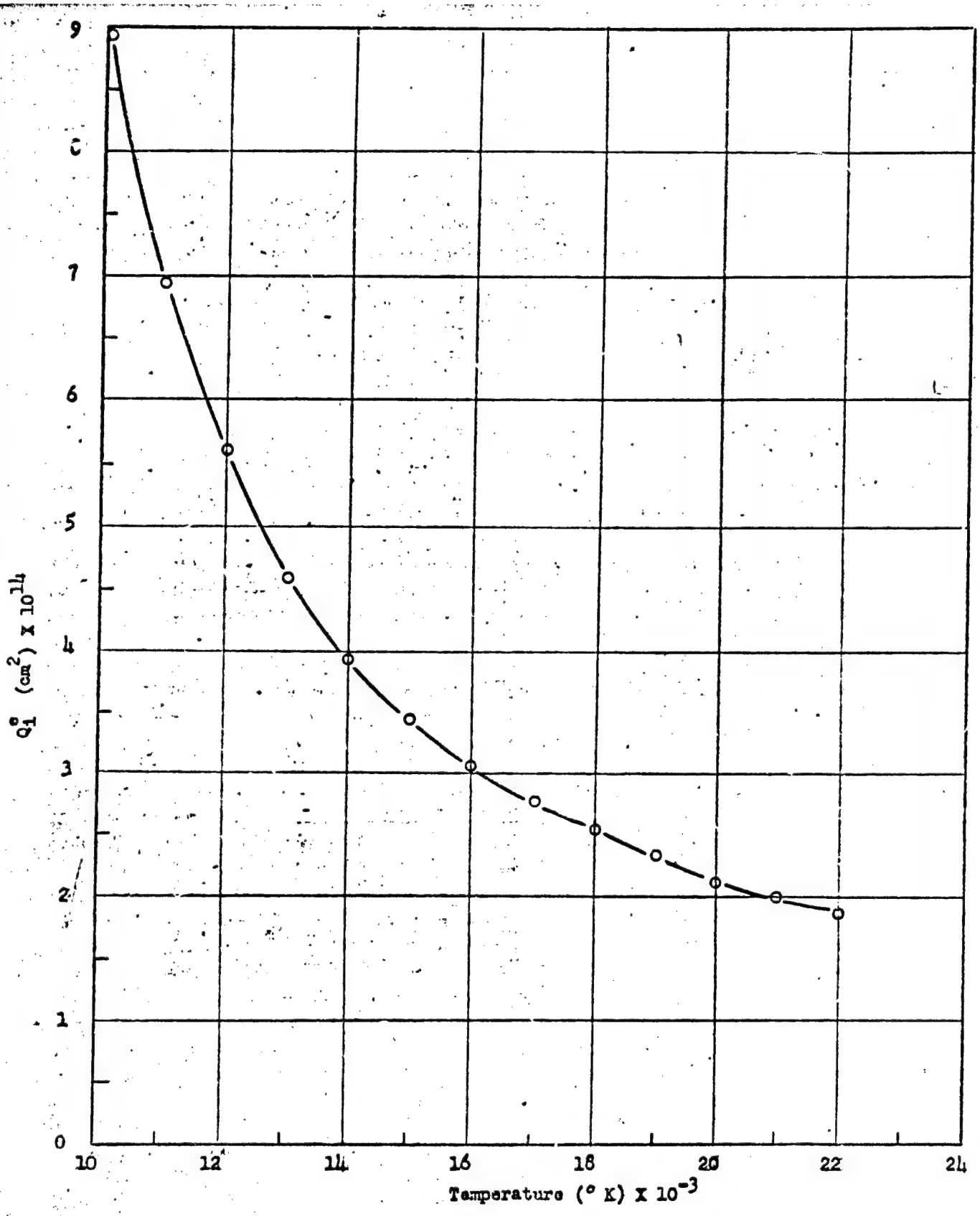

FIG. 9 ION-ELECTRON CROSS-SECTIONS FOR ARGON AT ATMOSPHERIC PRESSURE.

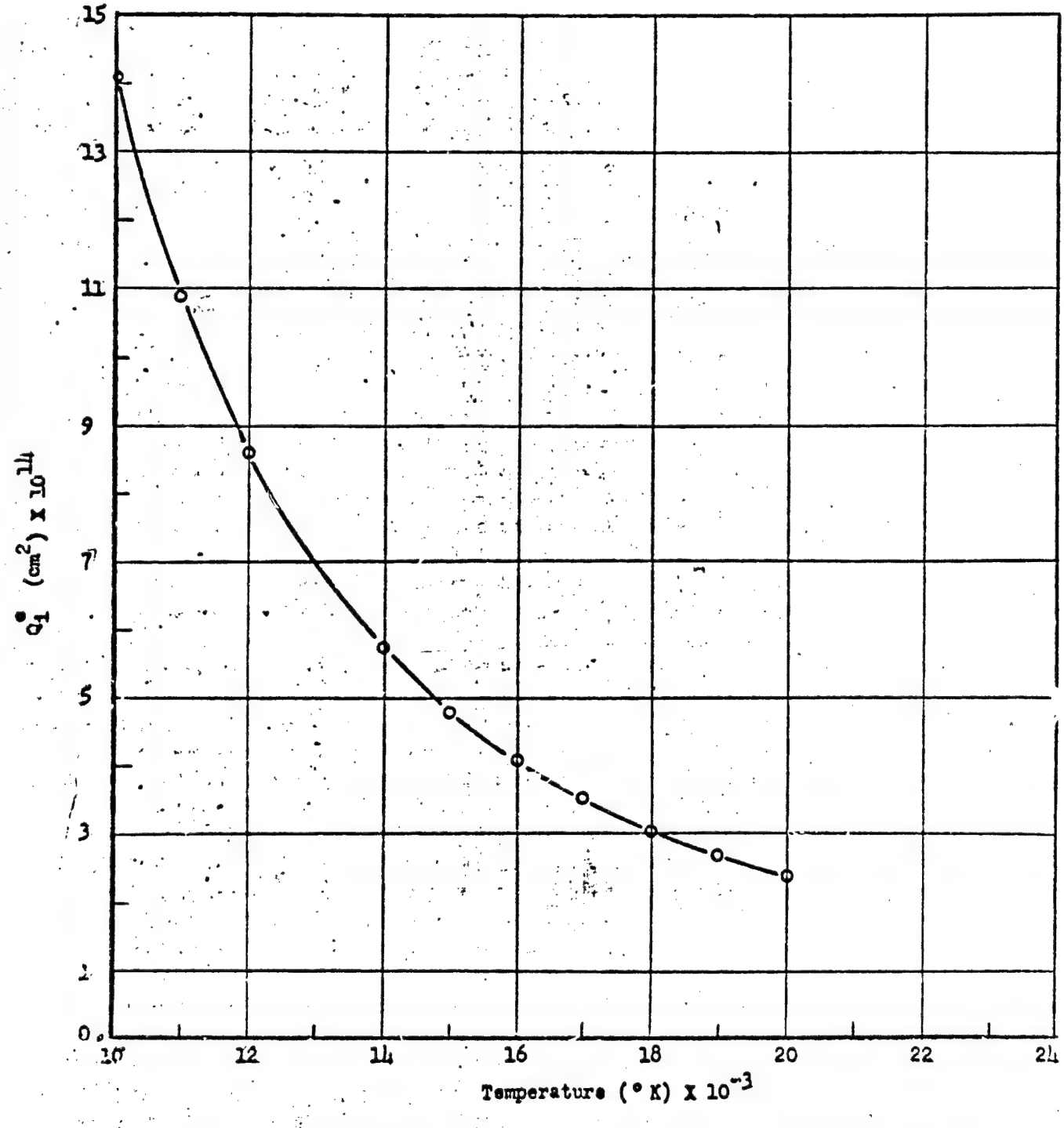

FIG. 10 ION-ELECTRON CROSS-SECTIONS FOR HELIUM AT ATMOSPHERIC PRESSURE.

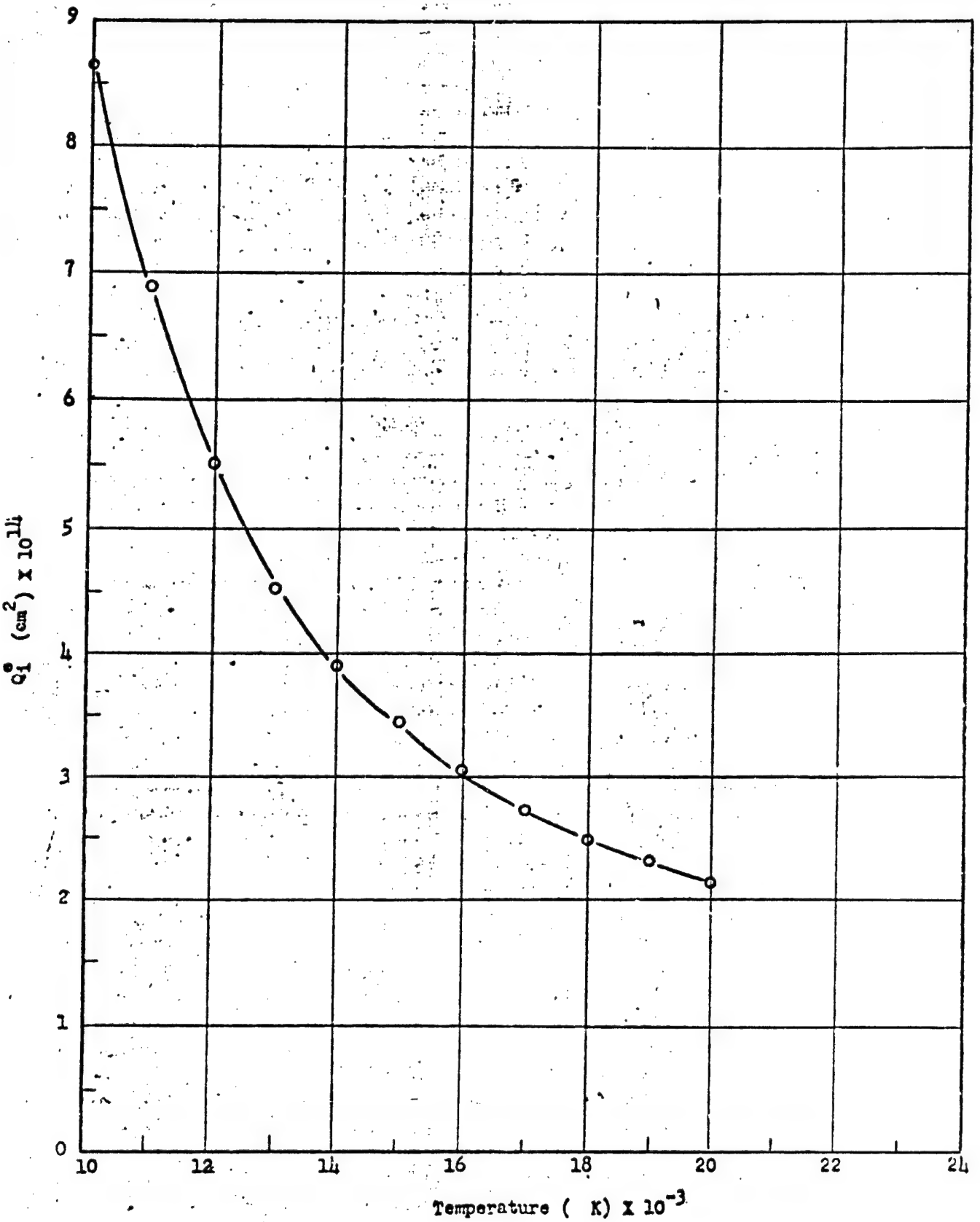

FIG. 11 ION-ELECTRON CROSS-SECTIONS FOR NITROGEN AT ATMOSPHERIC PRESSURE.

2.5 GENERAL COMMENTS ON SPECTROSCOPIC TEMPERATURE MEASUREMENTS

In recent years, with the advent of plasma physics studies in the laboratory, several new methods for making spectrometric measurements of high temperatures have been added to those which already had been developed by the astrophysicists. A review [16] of these methods shows the wide variety of techniques which are applied to different types of plasmas at different energy or temperature levels.

For our case, with a plasma at one atmosphere of pressure and at temperatures less than 25,000°K, the most likely methods involve the calculation of temperatures from measurements of intensity ratios of emitted spectral lines, from measurements of spectral line broadening caused by the emitting atom's collisions with other particles, or by making use of the radial intensity inversion of spectral lines emitted by cylindrical sources under certain conditions. Where necessary, these techniques will be described in some detail below. It is sufficient to say here that the choice of any one of these methods is determined largely by the ionization potential and type of spectra emitted by a particular element of interest. Any of these methods, of course, requires certain knowledge of spectroscopic quantities, such as energy levels, transition probabilities, line broadening coefficients, etc. In general, much of this information is lacking. However, recent work has been done for argon, nitrogen, and helium. In particular, the latest values for argon transition probabilities were obtained from H. N. Olsen [17], data on helium were obtained from W. B. Johnson [18] and A. T. Hattenberg [19], and nitrogen transition probabilities from data published by J. Richter [20].

Now in order to apply any of these techniques to measuring the temperature of an arc, it should be realized that a correction must be made when observing the intensity of radiation emitted from an optically thin cylindrical source. When observed from the side, the volume of such a source under observation is in the shape of a disk viewed edge-on. That is, an observer some distance from the side of this disk, when looking at a point on the arc surface, receives radiation emitted by many regions in the arc's interior behind this point. Since the depth of these regions is a function of arc radius, a relation must be used to transform the observed transverse intensity to a true radial intensity. Such a relation is the Abel integral equation,

$$I(x) = 2\int_{r=x}^{R} \frac{I(r)\, r\, dr}{r^2 - x^2} \quad , \tag{15}$$

where I(x) is the observed transverse intensity and I(r) is the true radial intensity. This procedure has been described in detail elsewhere [21], but for the sake of completeness, mention is made here of the fact that we had in the past used a numerical technique in obtaining I(r) as a function of I(x) from the relation

$$I(r_i) = \sum_{j=i}^{\infty} \alpha_{ij}\, I(x_j) \quad . \tag{16}$$

The coefficients in this relation, which are used in this present program for all the spectroscopic work, are given in Table 1.

Table 1. Values of a_{ij} Used to Transform Observed Int

i \ j	1	2	3	4	5	6	7	8	9	10	11	12	13	14	15
1	+.830818	-.8845.0	-.088354	.068530	.093107	-.314430	[illegible]	-.006103	-.004287	-.003871	-.003870	-.002412	.002035	-.001747	-.0015…
2		+.407043	-.354285	+.357036	-.048320	-.003851	-.212477	-.015088	-.004883	-.003581	-.002997	.002451	-.002080	-.001774	-.0018…
3			+.323343	-.376739	+.342182	-.036320	-.003431	+.004941	-.004378	-.004143	-.003080	-.002804	-.002151	-.001450	+.0018…
4				+.373740	-.353879	+.326737	-.031001	-.00.998	-.007723	.003732	-.003434	-.003706	-.003317	-.001936	-.0016…
5					+.344647	-.328380	+.033040	-.027307	-.001874	-.006871	-.003313	-.003260	-.002438	-.002057	-.0017…
6						+.332146	-.183656	+.030348	-.034000	-.001437	-.006340	-.003000	-.002970	-.002227	-.0018…
7							+.304994	-.172040	+.028232	-.033011	-.001232	-.006748	-.002757	-.002740	-.0030…
8								+.191128	-.160202	+.028816	-.021481	-.001116	-.003344	-.002867	-.0028…
9									+.178804	-.150812	+.028085	-.020198	-.001004	-.006016	-.0023…
10										+.170283	-.142301	+.023867	-.019029	-.000913	-.0047…
11											+.162130	-.139484	+.022812	-.018166	-.0006…
12												+.158046	-.130448	+.021867	-.0172…
13													+.148816	-.126168	+.0210…
14														+.143263	-.1104…
15															+.1283…
16															
17															
18															
19															
20															
21															
22															
23															
24															
25															

$c_{I_i} = \sum_{j=1}^{25} a_{ij}\, {}^{o}I_j$

dial Intensities*

18	19	20	21	22	23	24	25
-.001138	-.000971	.000837	.000757	-.000699	.000629	-.000578	-.000531
-.001050	-.000938	-.000843	.000[illegible]43	-.000693	[illegible]	-.000579	-.000532
[illegible]	-.000956	-.000857	-.000774	-.000703	-.000640	-.000586	-.000538
[illegible]	.000981	-.000876	-.000791	-.000718	.000653	-.000594	.000546
-.00[illegible]50	-.001018	-.000908	-.000813	-.000736	-.000668	-.000606	-.000560
-.00[illegible]112	-.001067	-.000946	.000846	-.000761	-.000689	-.000627	-.000572
-.001298	-.001130	.000998	-.000887	-.000794	-.000716	-.000648	-.000591
-.001400	-.001217	-.001062	.000938	-.000836	.000746	-.000676	-.000614
-.001540	.001319	-.001147	-.001003	-.000887	-.000791	-.000711	-.000642
-.001703	-.001462	-.001248	-.001088	-.000852	-.000843	.000752	-.000676
-.002148	-.001617	-.001408	-.001180	-.001036	-.000907	-.000804	-.000716
-.002026	-.002040	-.001542	-.001344	-.001134	-.000990	-.000867	-.000768
-.004118	-.001928	-.001961	-.001476	-.001267	-.001087	-.000948	-.000832
-.000674	.003966	-.001800	-.001883	-.001417	-.001238	-.001044	-.000917
-.015473	-.000494	-.002811	-.001787	-.001613	-.001364	-.001191	-.001006
+.219072	-.014867	-.000890	-.002092	-.001722	-.001750	-.001316	-.001190
-.108087	+.018524	-.014807	.000548	-.003566	-.001664	-.001683	-.001373
+.128066	-.104867	+.018031	-.014086	-.000640	-.003466	-.001611	-.001641
	+.122638	-.102083	+.017869	-.013703	-.000818	-.003790	-.001363
		+.119486	-.093444	+.017126	-.013347	-.000498	-.003270
			+.116844	-.096990	+.016727	-.013018	-.000472
				+.113646	-.094710	+.016264	-.012712
					+.111310	-.092853	+.019004
						+.108837	-.090884
							+.106760

The spectrograph used in this work was a 3.4 meter Ebert-type stigmatic instrument having a plane grating with 6000 lines/cm and 15 cm of ruling. The theoretical resolving power of the instrument is 100,000 with a linear dispersion of 5 Å/mm in the first order. The critical slit width for the instrument is 12μ at 5000 Å, which gives rise to very low instrumental line broadening and allows detailed examination of spectral line shapes. The arc was imaged on the slit with an achromatic lens. In addition, a Dove prism was used to rotate the arc image by 90 degrees, so that the arc axis was perpendicular to the entrance slit of the spectrograph. All of the work being reported here was done photographically, with the optical density of the spectral plates recorded by a scanning microdensitometer. A standard tungsten strip lamp and rotating sector were used for photographic plate calibration.

Self-absorption in the arc plasma was checked by using a concave mirror to reflect some of the light of the arc back through the arc a second time. Additivity of intensities indicates the absence of self-absorption, and this method provides a simple, convenient check for such absorption.

2.6 SPECTROSCOPIC TEMPERATURE MEASUREMENTS

2.6.1 Argon

Since temperatures and degrees of excitation were previously unknown in our arc, a survey of all argon spectral lines in the visible and near infrared was made initially for purposes of line identification and to qualitatively estimate intensity ratios within these lines. Fifteen atomic lines with known transition probabilities were

identified in the region λ6500 to λ9000 Å and two ionic lines with known transition probabilities in the region λ3700 to λ4300 Å. No impurity lines were definitely observed. An electron continuum was apparent in a portion of the spectral region.

Of the choices available for measuring the temperature of the argon arc, the radial intensity inversion technique was chosen as being most appropriate. The discussion in section 2.7 will demonstrate that some uncertainty may exist in the transition probability data and thus possibly invalidate temperatures which would be obtained by using line intensity ratios.

The λ8264 argon line, after being tested for self-absorption, was chosen for the temperature measurements. The energy of the upper energy state giving rise to this transition is 13.3 ev. A plot of the intensity-temperature distribution of this λ8264 line (as computed by using the atom number densities and the Boltzmann factor) is given in Figure 12. As can be seen, the temperature for which the intensity of this line is a maximum is approximately 15,300°K. Thus, if the plasma temperature on the axis of the arc exceeds this value, a distribution of the intensity of this line as a function of arc radius will exhibit a maximum, which corresponds precisely to a temperature of 15,300°K. Once this point is established, a complete radial temperature profile can be easily established by comparing the relative intensities as a function of temperature in Figure 12 to the relative intensities as a function of arc radius as obtained spectrographically.

It was found, after several trials, that an argon arc operating at 270 amps showed a pronounced off-axis intensity peak. The data were obtained with the spectrographic slit optically aligned

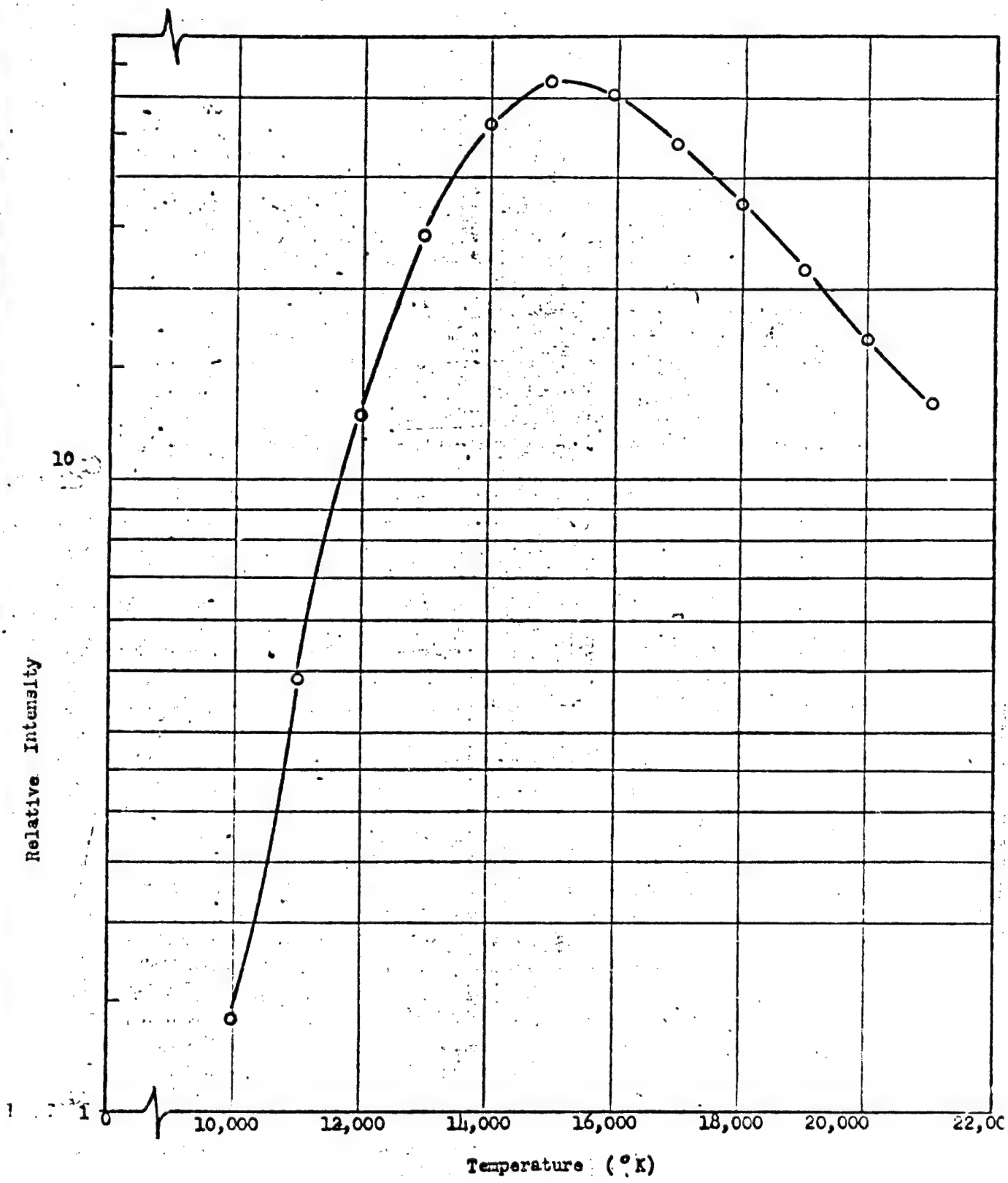

FIG. 12 CALCULATED INTENSITY-TEMPERATURE DISTRIBUTION OF THE ATOMIC λ8264 SPECTRAL LINE IN ARGON.

transverse to the arc itself, so that the height of any spectral line as it appeared on the photographic plate corresponds to a radial view of the arc at a distance of several millimeters above the anode in a 3/8-inch long arc. A 200μ entrance slit width was used with exposure times varying from 1/100 to 1/5 of a second. A microdensitometer record of the intensity versus height along the spectral line provided a measure of the intensity as a function of transverse distance across the arc. Using the Abel integral equation and the coefficients given in Table 1, a measure of the intensity versus arc radial distance was obtained. Converting this information to temperature (using Figure 12) resulted in the radial temperature distribution for the argon arc as given in Figure 13.

2.6.2 Helium

The problem of measuring temperatures in a helium plasma proved considerably more difficult than originally anticipated. First of all, the only transition probability data in the visible exist for spectral lines with upper energy states between 21 and 23 ev. This narrow range scarcely provides the sensitivity required for using line intensity ratios. This method could be used if one could get down to the 600 Å region or use an ionic line. However, we were not equipped to do spectroscopy in the ultraviolet, and no ionic lines were observed in our spectra.

However, since we had data on helium plasma composition and spectral line broadening [18, 19], and since our spectrograph had sufficient dispersion and resolution to examine line shapes, we considered the procedure for relating line broadening to electron density and temperature. The best diagnostic spectral lines appeared to be the

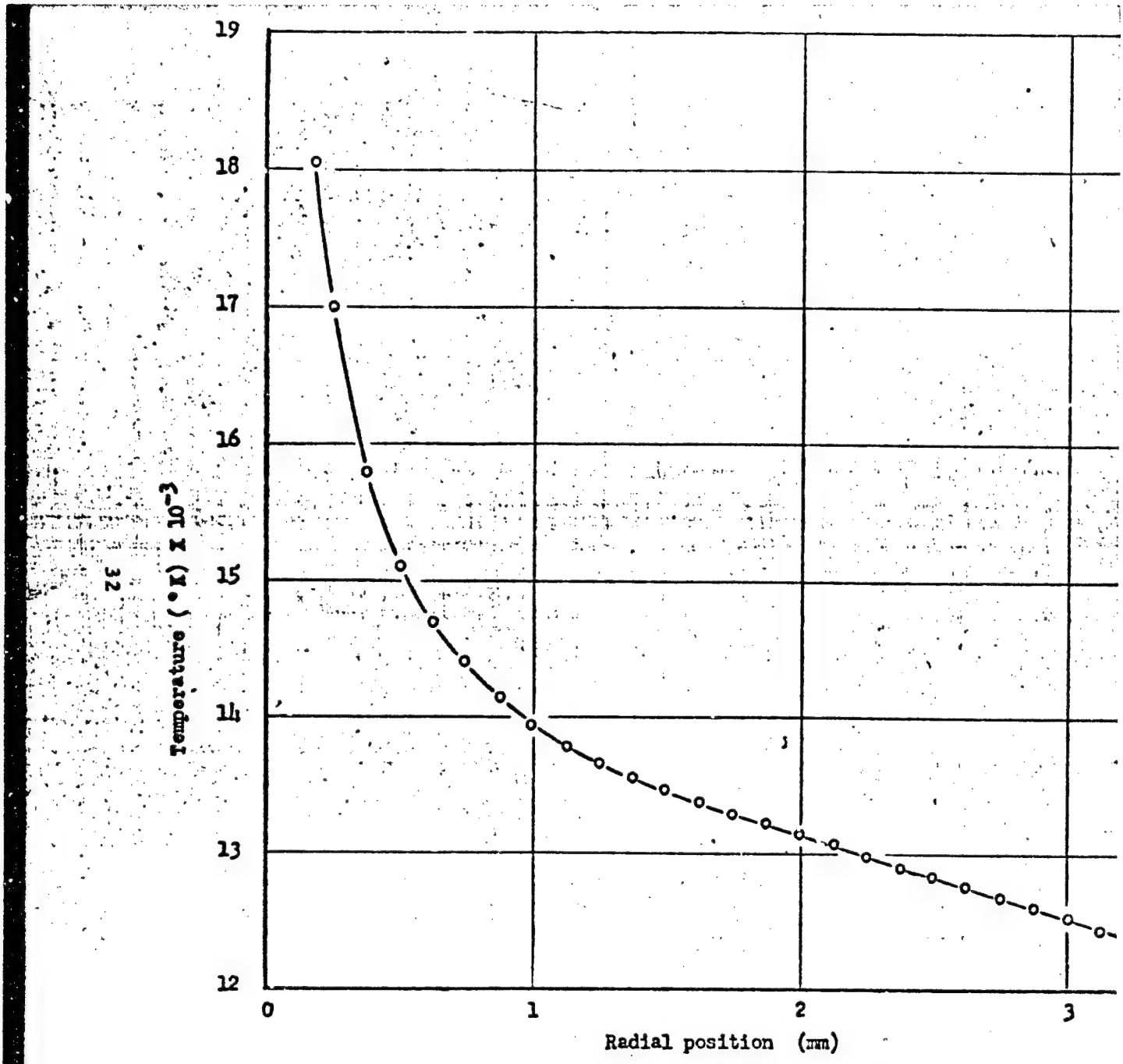

FIG. 13 TEMPERATURE vs RADIUS IN A 270-AMPERE ARGON ARC ABOVE ANOD

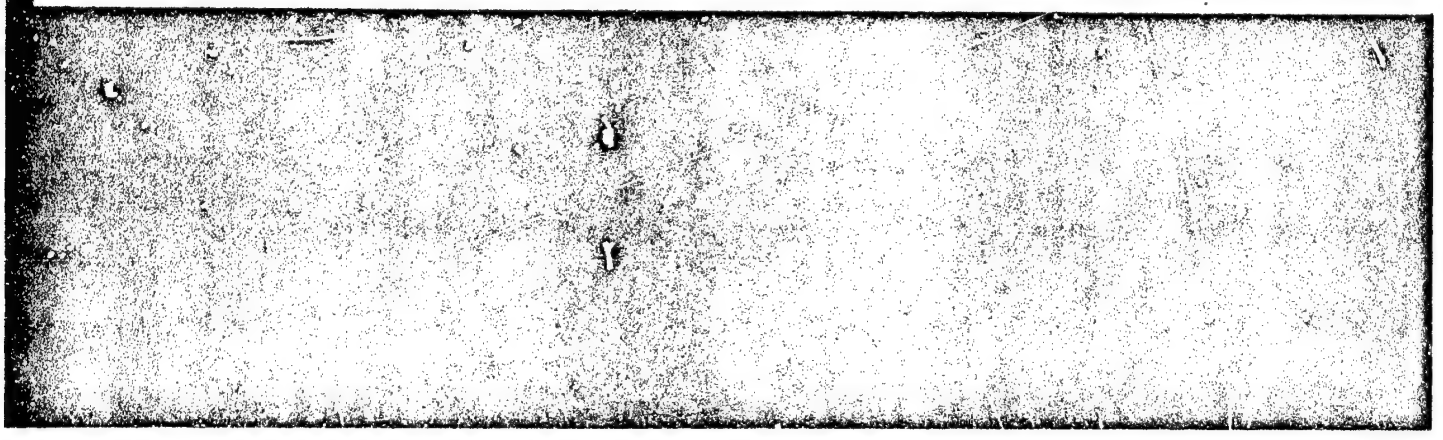

A

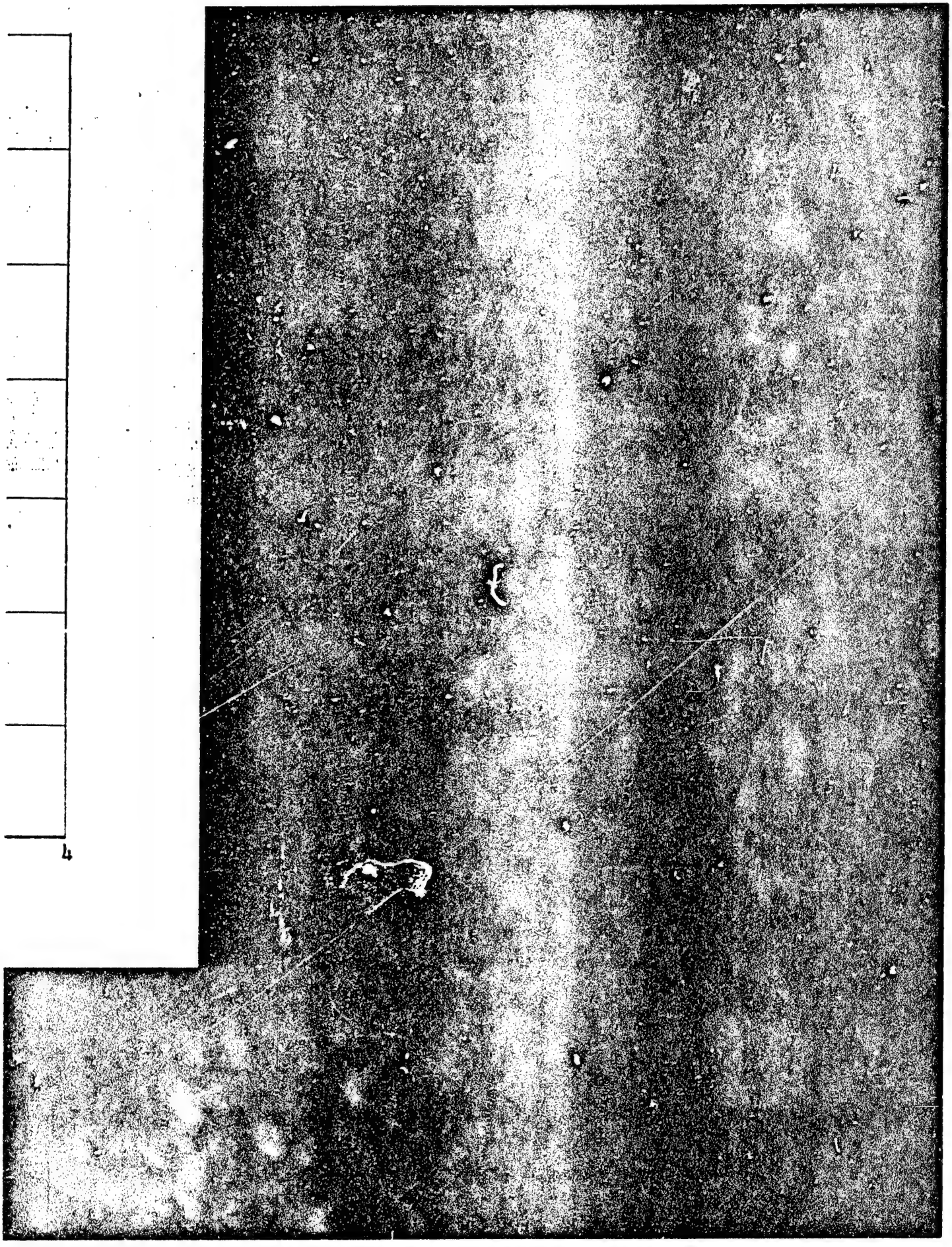

B

λ5015 and λ4713, since they both have fairly large shifts and widths, are approximately symmetrical in wavelength, and are reasonably strong lines.

After considerable preliminary work, observations were made of the λ5015 line using the second order dispersion for an arc current of 230 amps. A 10-micron entrance slit was used, and again a transverse view of the arc above the anode was exposed along the length of the slit. After plate exposure and processing, a fine line, parallel to the spectral lines, was scribed on the plate to provide a reference from which wavelengths corresponding to the spectral line originating from different parts of the arc could be accurately correlated. In this way, line shifts as well as widths could be determined as a function of arc radius. Once again, of course, the Abel inversion process was required to correct the observed transverse intensity to a true radial intensity.

The theory used was that of Griem, which had been confirmed experimentally by Berg [23], and which relates the electron density in a helium plasma to the width and wavelength shift of the neutral helium spectral lines, even in the absence of LTE. In this theory, the width at half-height and the wavelength shift of the line peak are linear functions of the electron density and vary only slightly with electron temperature. For the λ5015 line, the electron density $n_e = 1.14 \times 10^{16} \Delta\lambda_{1/2}$, where $\Delta\lambda_{1/2}$ is the full width at half-maximum in angstroms, and $n_e = 3.89 \times 10^{16} \Delta\lambda$, where $\Delta\lambda$ is the wavelength shift of the intensity maximum in angstroms.

Examination of the data revealed that our half-width measurements appeared consistent and reliable but that the wavelength shift measurements were unsatisfactory due to the inability of our

microdensitometer-recorder system to accurately determine absolute wavelength. The half-width data, then, provided electron density which was converted to temperature by the use of Saha's equation. As it turned out, a temperature variation of less than 1000°K was measured across the portion of the arc which was exposed spectrographically. Since time did not permit the rather extensive data reduction procedure which would have been required for additional exposures of the helium arc, data for this gas is given only for a temperature of 15,000°K (that measured by the line-broadening technique).

2.6.3 Nitrogen

As described above, nitrogen gas was mixed with argon to provide an atmosphere in which electrode erosion could be eliminated. The arc was operated with the nitrogen component as large as possible (commensurate with this electrode condition) to provide maximum sensitivity when comparing properties of this argon-nitrogen arc to the pure argon arc.

After variations of gas ratios and arc current had been investigated, spectral plates were exposed using an arc current of 350 amps with a gas ratio of 66 per cent argon, 34 per cent nitrogen. As in the case of pure argon, a 200-micron entrance slit width was used with exposure times between 1/100 and 1/10 of a second. Also the λ8264 line in argon was once again used for the temperature determination with a correction being made for the change in argon atom density as a function of temperature. Using the same process of applying Able's integral equation and transforming the observed transverse intensity to a true radial intensity, the temperature versus arc radius distribution shown in Figure 14 was obtained.

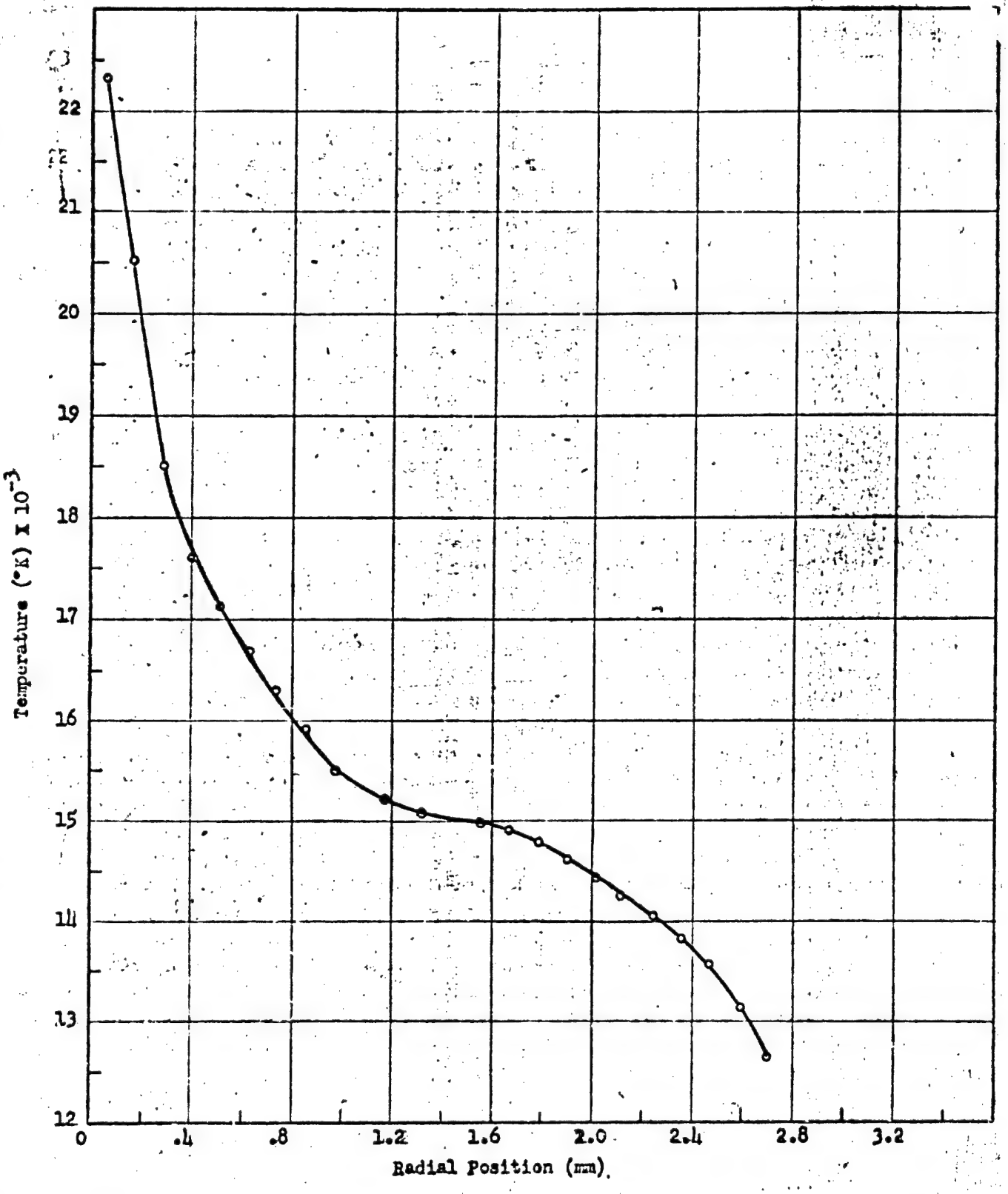

FIG. 14 TEMPERATURE vs RADIUS IN 350-AMPERE,, 34% NITROGEN, 66% ARGON ARC ABOVE ANODE SURFACE.

2.7 SPECTRAL LINE SHAPES IN ARGON

Quite unexpectedly, a seemingly curious condition was found to exist concerning the shapes of atomic argon spectral lines. Of the fifteen lines in the region λ6500 to λ9000 Å, several show a strong shift of the intensity peak to the red along with a pronounced dip on the blue side of the line, while others are relatively unaffected. A typical example of a line exhibiting such characteristics is shown in Figure 15. The slit width used here was 10 microns, providing an instrumental line width of less than 0.05 Å. This condition is not present at arc currents of 50 amps, begins to appear between 100 and 200 amps, and is fully developed at 250 amps. Although this situation did not affect our measurements, it is of some interest for its own sake. It is mentioned here for the sake of completeness and to make it more generally known to workers in the field.

It initially seemed strange that some lines were affected and others not, since all of the lines mentioned have about the same upper energy state ($\approx$ 13 ev) and about the same lower energy state ($\approx$ 11 ev) and, further, there exists no correlation with the atomic configurations of the energy states giving rise to these transitions. There was further no correlation between the affect and the latest published values for argon transition probabilities [16] .

A literature search was made at this point, and it became apparent that there were many instances of argon lines being shifted rather strongly to the red. This shift is in general caused by the interaction of the emitting atom with the surrounding charges in the plasma and is directly proportional to the electron density. This explains the dependence of the line profile on the current, since the electron

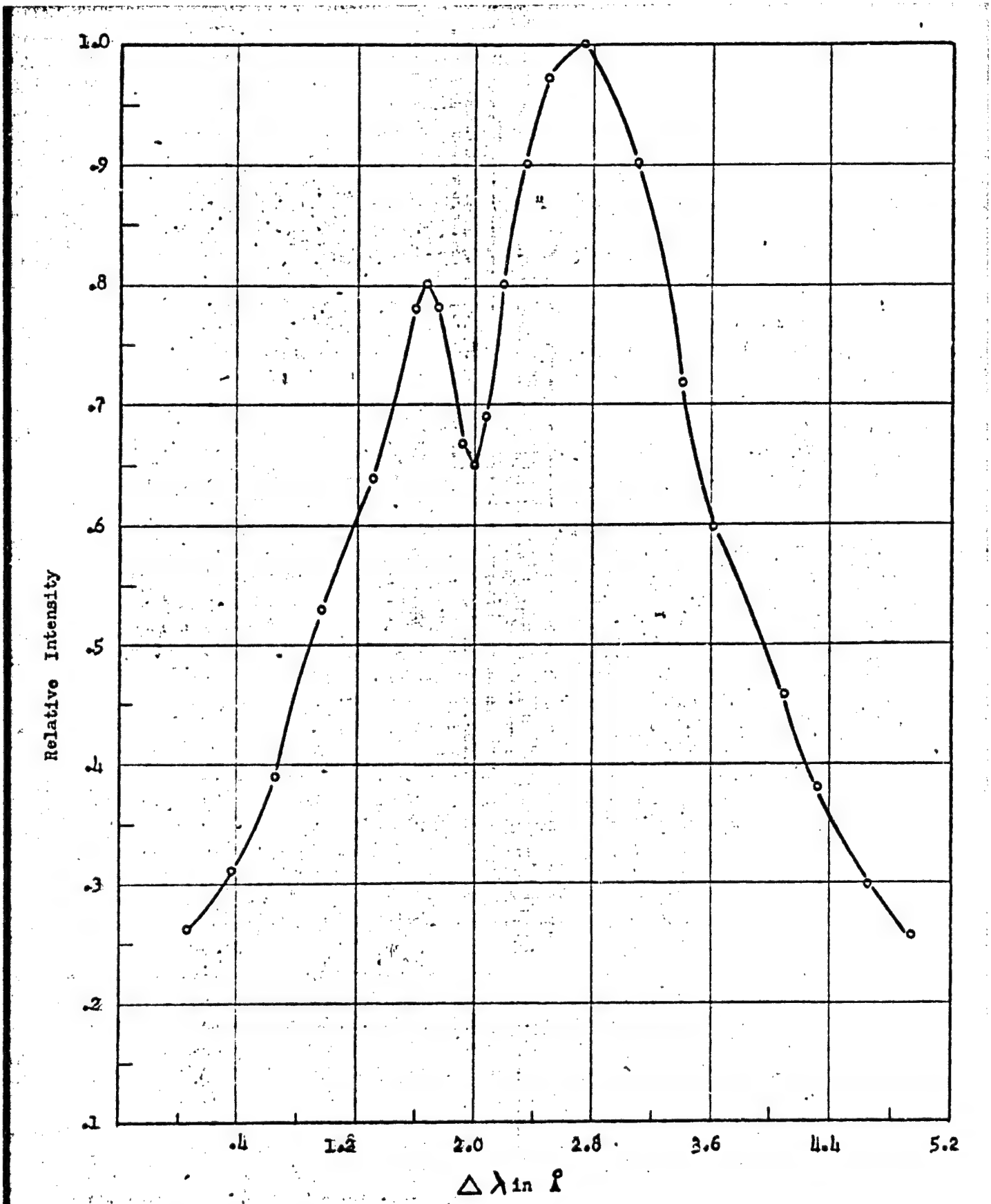

FIG. 15 PROFILE OF THE λ 8115 LINE IN AN ARGON ARC AT 200 AMPERES

density depends on the arc current. The dip in the curve has been assumed to be due to absorption of radiation in cooler layers surrounding the hottest part of the arc. A calculation of the radiation flux from the axis of the arc through the absorbing layer suggests that absorption can be appreciable if the absorbing layer is about 1 mm in thickness. It is strange that absorption should occur from a level lying more than 11 volts above the ground state, but calculations also show that this is possible.

In the case that absorption is actually responsible for the dip in the lines, those lines with larger transition probabilities should be absorbed more strongly. It has been mentioned here that no such correlation was observed with the latest values for transition probabilities. However, previous values [24] do show a good correlation, so the possibility exists that these initial values are actually the correct ones and later values may be in error. More work should be done to substantiate this inference based on these line broadening observations.

One further interesting point is that some crude approximations were made using our line profiles and the only data [25] found in the literature which was applicable. The shift in the intensity peak of the λ8115 line corresponds roughly to an electron density of about $1.7 \times 10^{17}/cm^3$, or a temperature of about 15,000°K. The shift of the intensity dip indicates the absorbing layer was at a temperature of about 11,000°K. These temperatures are in agreement with those obtained by the intensity inversion of the λ8364 line as shown in Figure 12.

2.8 ELECTRIC FIELD DETERMINATIONS

The electric field in the arc plasma was determined for each particular case of interest by measuring the total voltage across the arc and subtracting from this the sum of the electrode drops. The electrode drops in an atmospheric pressure arc can be determined with reasonable accuracy by plotting the total arc voltage as a function of arc length and then extrapolating the curve back to zero length. The point where the curve intercepts the voltage axis is then the sum of the anode and cathode drops. Data for the three gases are given in Figures 16, 17, and 18 for the arc currents at which spectroscopic data were obtained in each case.

2.9 RADIAL CURRENT DENSITY DISTRIBUTIONS

In order to measure current densities as a function of arc radius, a special anode was fabricated with a probe inserted directly at the center (see Figure 19). This probe, 0.040 inch in diameter, is mounted in a conventional anode plate and insulated from the rest of the structure so that fractional amounts of current to the probe and the anode surface can be measured.

In its design, one has to consider such problems as resolution, electrical insulation, and cooling. The probe tip must be of small diameter to insure that a great number of readings can be taken over the total diameter of the arc. Good resolution is necessitated by the fact that values of current density may change by three orders of magnitude within a radial increment of 2 mm.

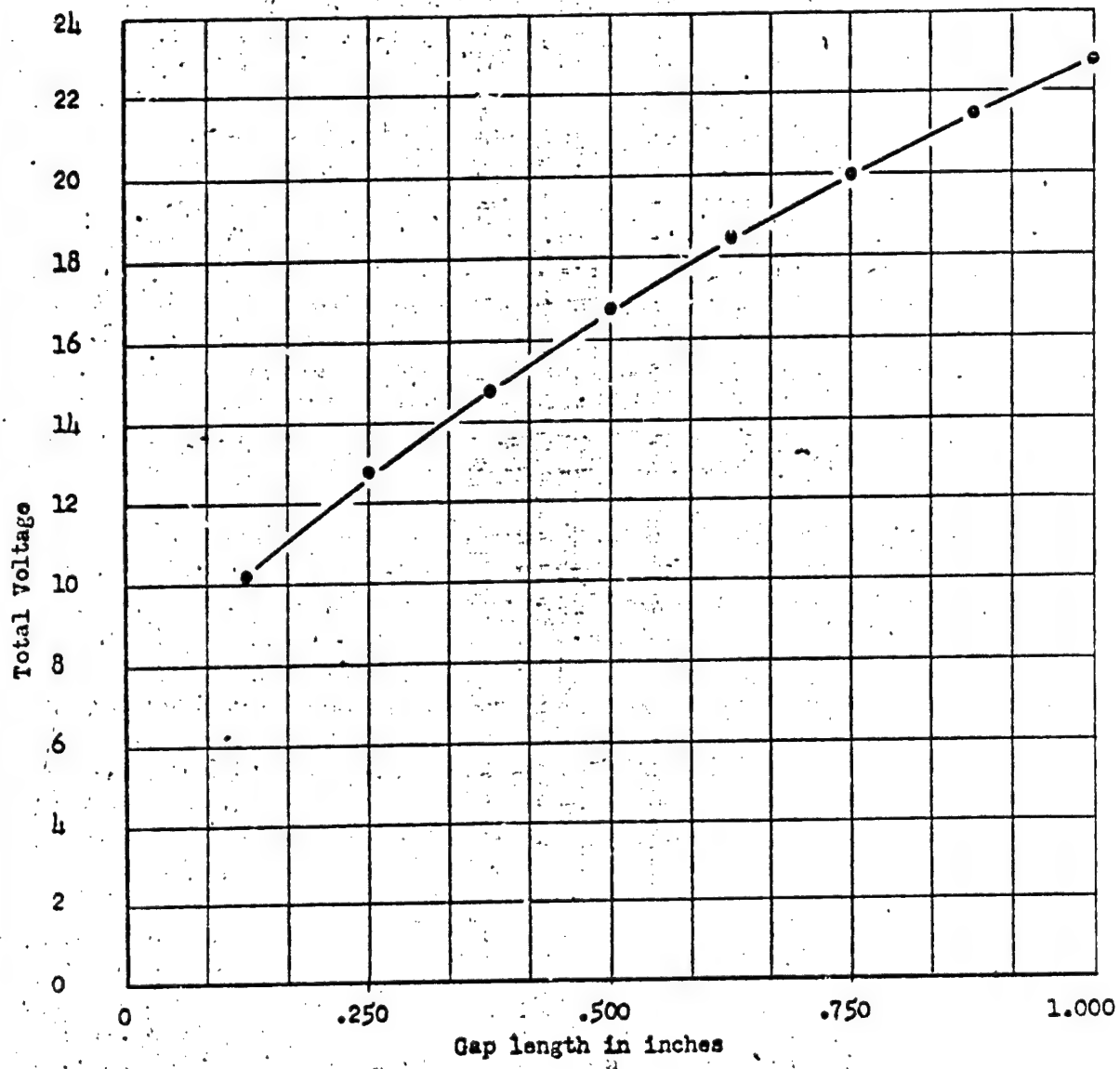

FIG. 16 ARC VOLTAGE vs LENGTH FOR 270 AMPERES IN ARGON

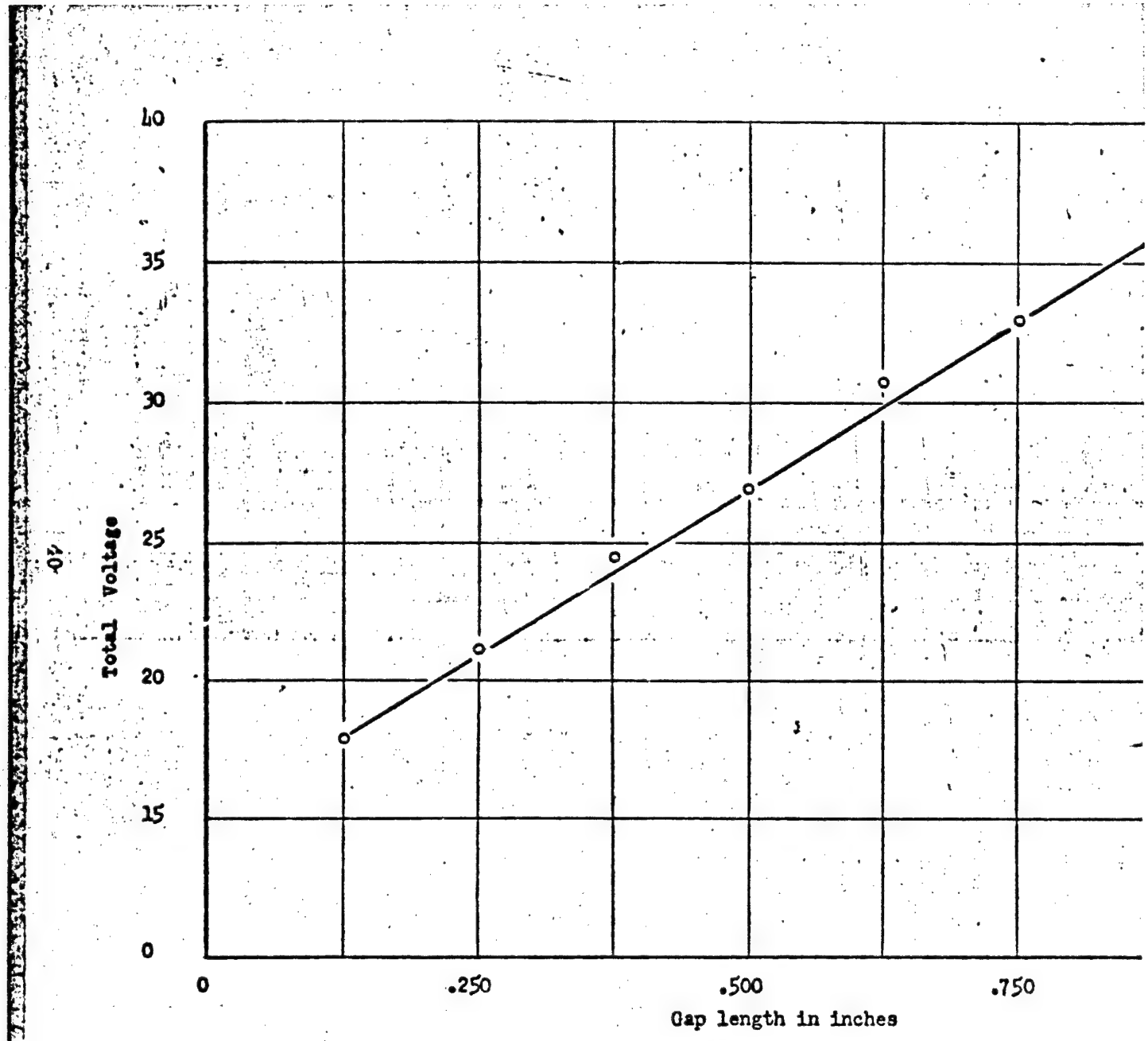

FIG. 17 ARC VOLTAGE vs. LENGTH FOR 230 AMPERES IN HELIUM

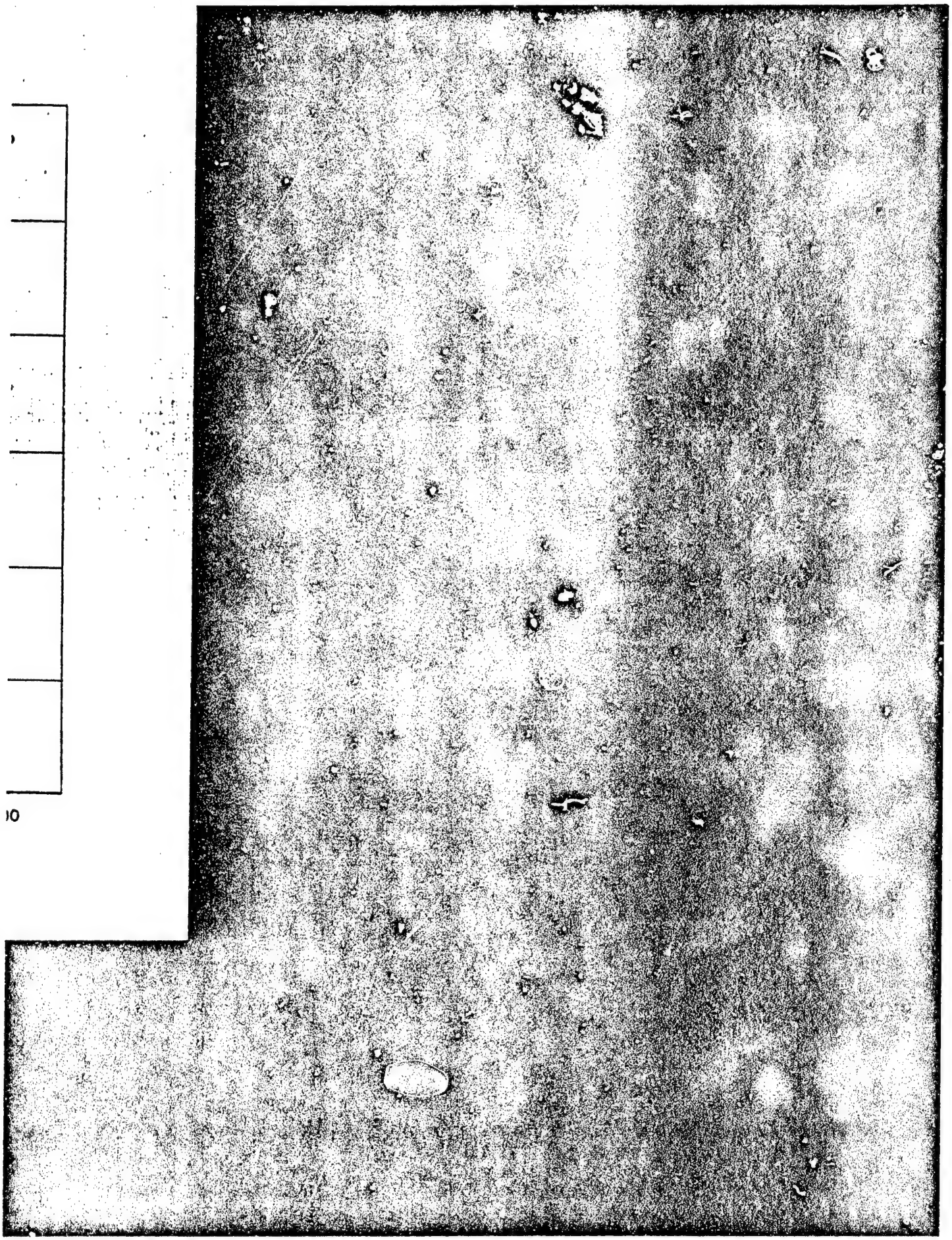

B

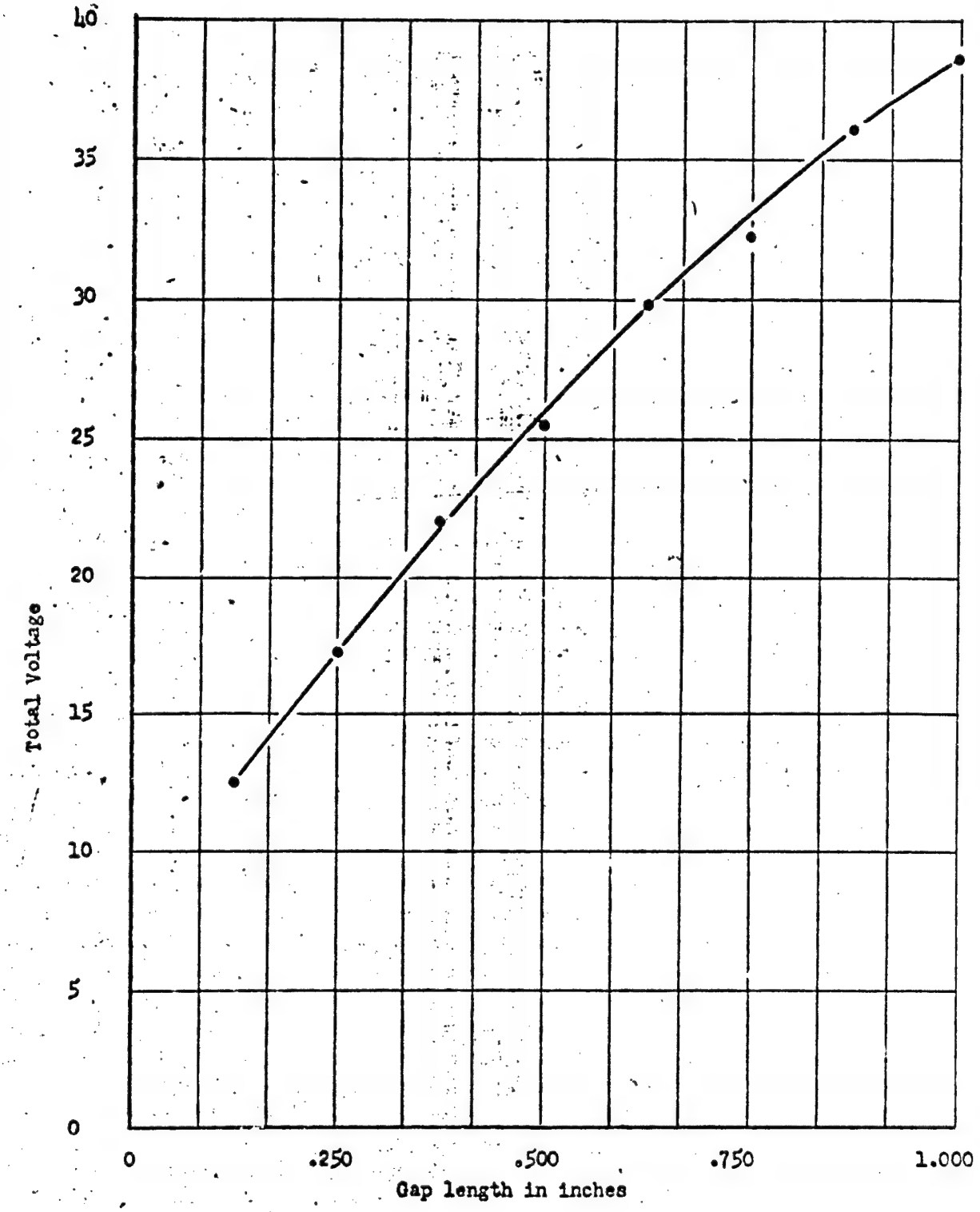

FIG. 18 ARC VOLTAGE vs LENGTH FOR 350 AMPERES IN 66% ARGON, 34% NITROGEN

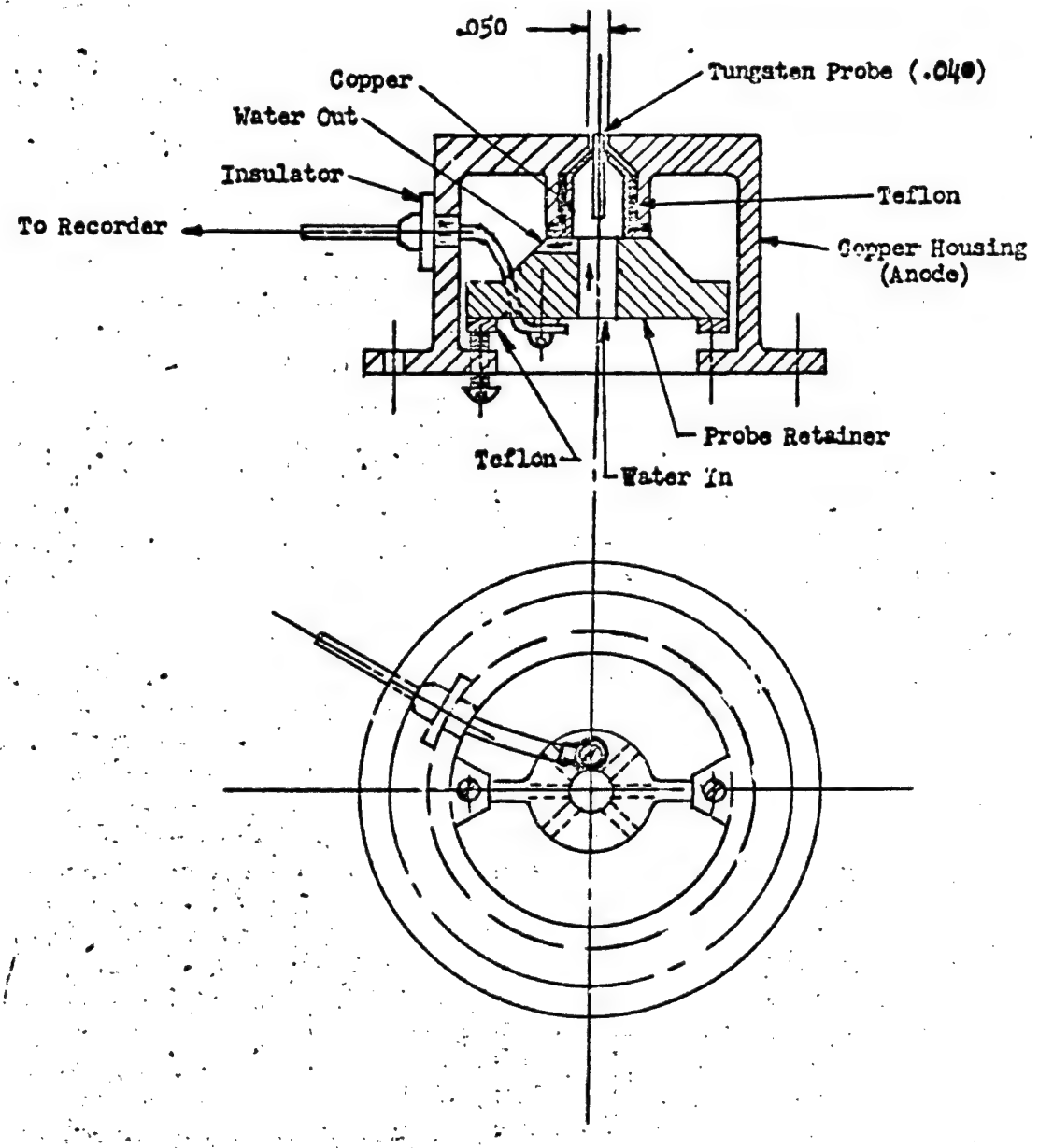

FIG. 19 SCHEMATIC OF THE CURRENT PROBE-ANODE

Since the probe tip must be electrically insulated from the rest of the anode, its assembly alone must conduct the heat to the cooling water below. At the center of symmetry of the arc, the current density is a maximum, and probe diameter must be of sufficient diameter to thermally conduct the heat generated at the surface of the probe as well as the joule heat generated within the probe by the high current densities. Consequently, the probe tip was made as short as possible and was fitted into a copper cone which presented a much larger area to the cooling water than could the probe tip alone.

While the probe tip and the rest of the anode are not electrically connected by a metal, they are connected by the cooling water. However, since both tip and rest of the anode are at the same potential, except for second order inhomogeneities in the field, the leakage current between the two is extremely small and completely negligible.

By moving the entire anode structure in a direction transverse to the arc column, the probe measures current as a function of arc radius, which can easily be transformed to current density. Data were always checked by integrating the current density curve thus obtained and comparing it with an independent total current measurement.

Figure 19 shows that the anode cooling water may be expected to be as effective as in the case of the regular anode, except in a small region immediately surrounding the probe. Initial testing of the unit showed perfectly satisfactory operation in helium and argon arcs, with no erosion occurring at either the probe or the rest of the anode surface. To obtain data, then, the anode was simply cranked by hand across the arc, and probe current was read using a series of ammeters (see Figure 20a

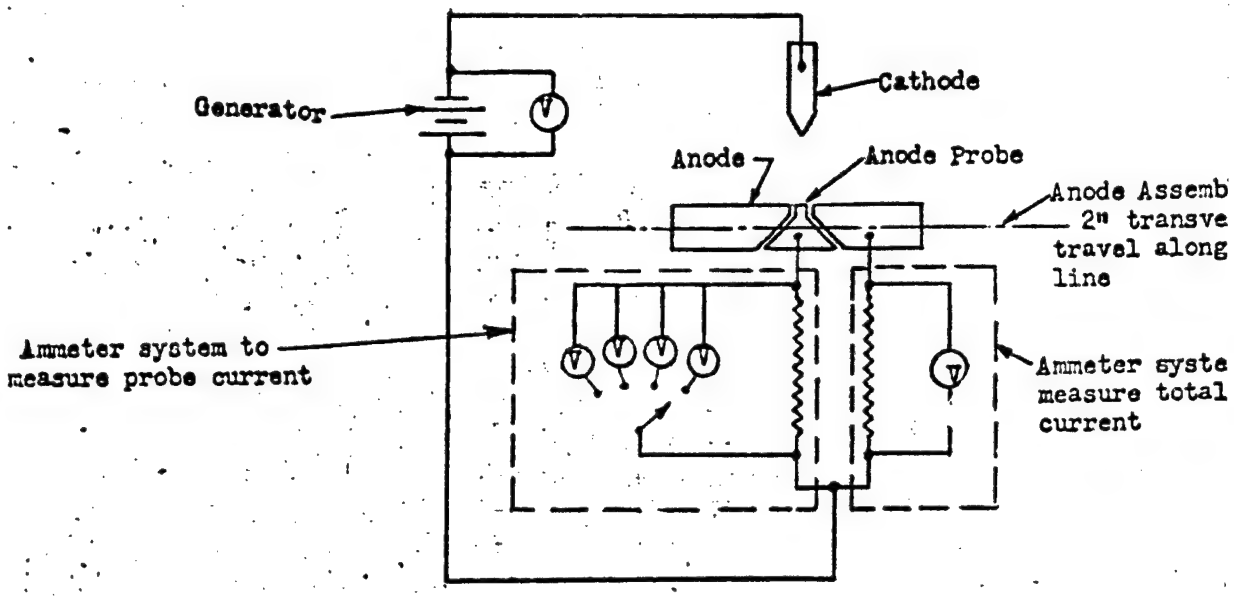

FIG. 20(a) CIRCUITRY USED WITH CURRENT PROBE-ANODE IN ARGON AND HELIUM

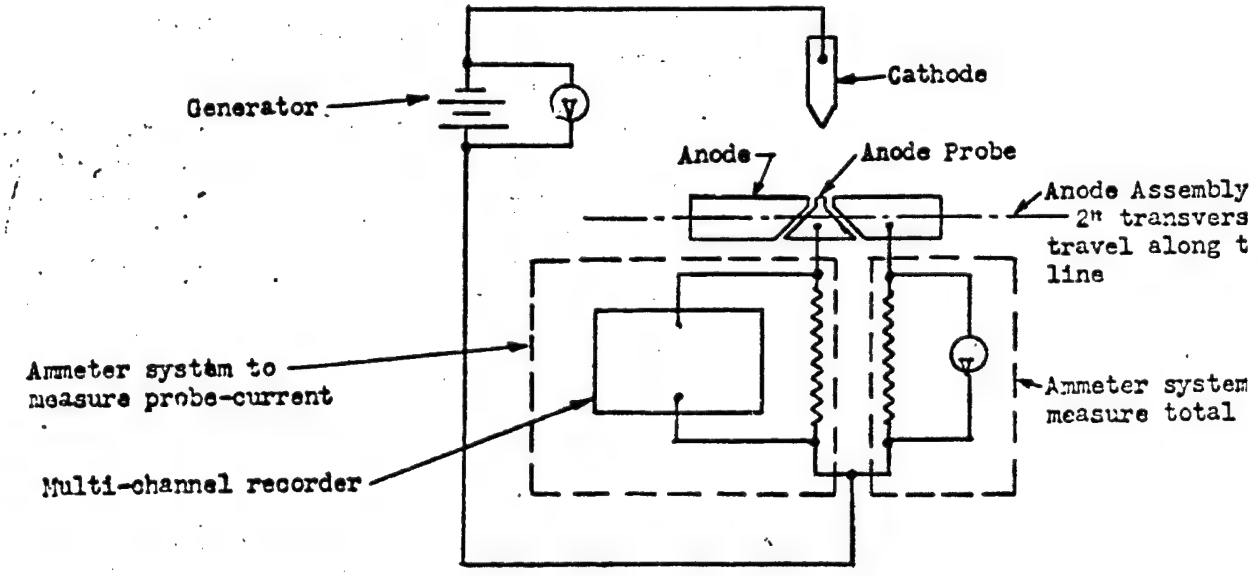

FIG. 20(b) CIRCUITRY USED WITH CURRENT PROBE-ANODE IN NITROGEN-ARGON MIXTURE

However, for the case of the argon-nitrogen arc, the effect of the higher current (350 amperes versus 270 or 230 amperes) along with the deleterious effect of nitrogen on electrode surfaces resulted in a series of failures due to erosion in the immediate vicinity of the probe. This situation was remedied by using an electric motor-gear box assembly which moved the anode across the arc at a rate of 5 inches/minute. The time the probe spent near or in the hot central portion of the arc was thus much reduced, and no erosion occurred. A multi-channel recorder was used in this case to record the probe current as a function of arc radius (see Figure 20b). Current densities measured with this technique are shown in Figures 21, 22, and 23 for argon, helium, and argon-nitrogen, respectively.

3. RESULTS

3.1 CROSS SECTIONS

Equation (8) in section 2.2 forms the basis for our atom-electron cross section determinations. Rewriting this expression, we have that the atom-electron collision cross section Q_e^a is given by the relation

$$Q_e^a = \frac{1}{n_a} \left\langle \frac{e^2}{\left(\frac{8mK}{\pi}\right)^{1/2}} \frac{n_e E}{J T^{1/2}} - n_i Q_e^i \right\rangle \quad . \qquad (17)$$

We have seen in the previous discussion how the electric field E, the current density J, and the temperature T were experimentally measured in arcs operating in argon, helium, and a known mixture of argon and nitrogen. Further, the electron, ion, and atom number densities

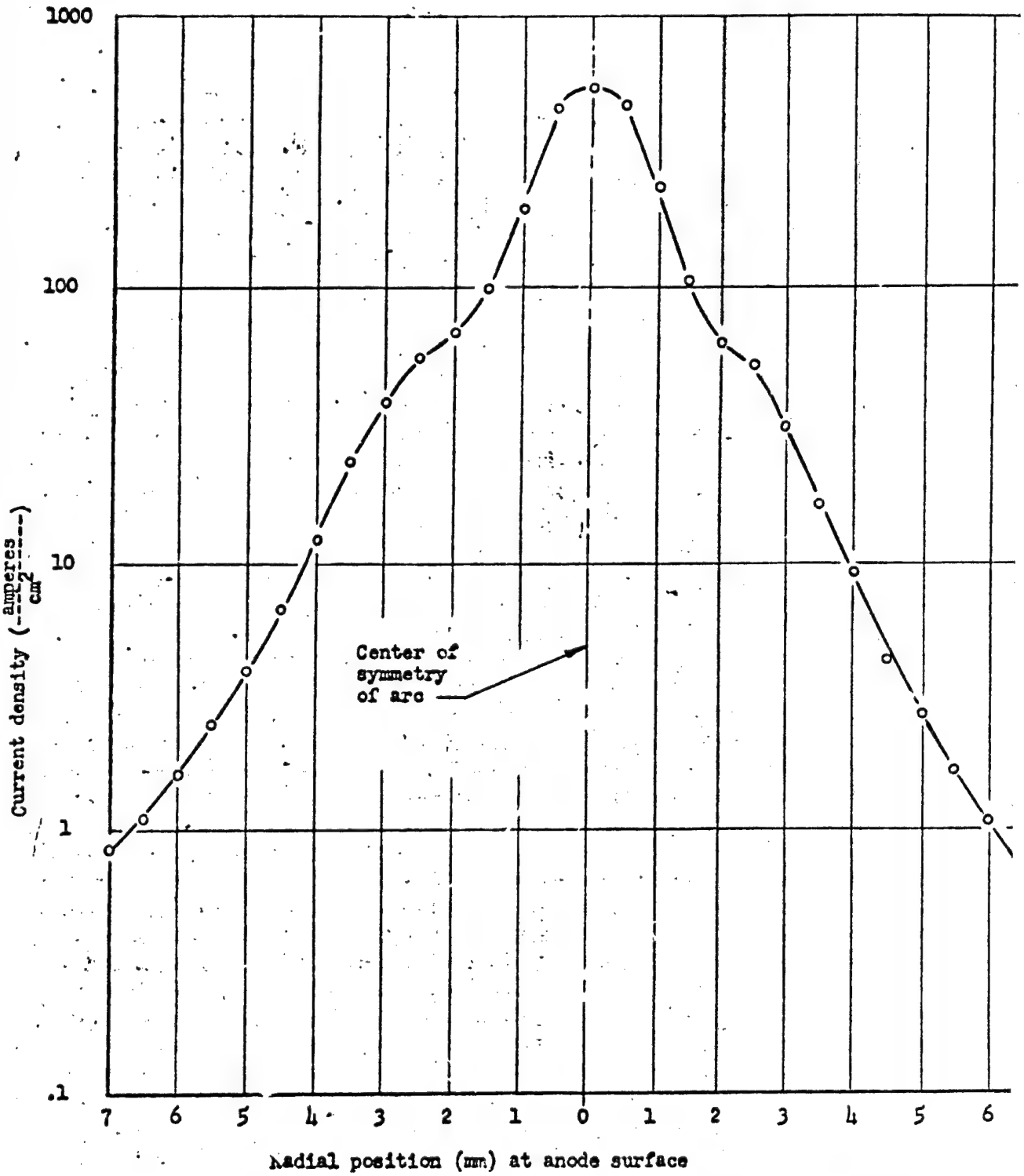

FIG. 21 CURRENT DENSITY vs ARC RADIUS IN AN ARGON ARC AT 270 AMPERES

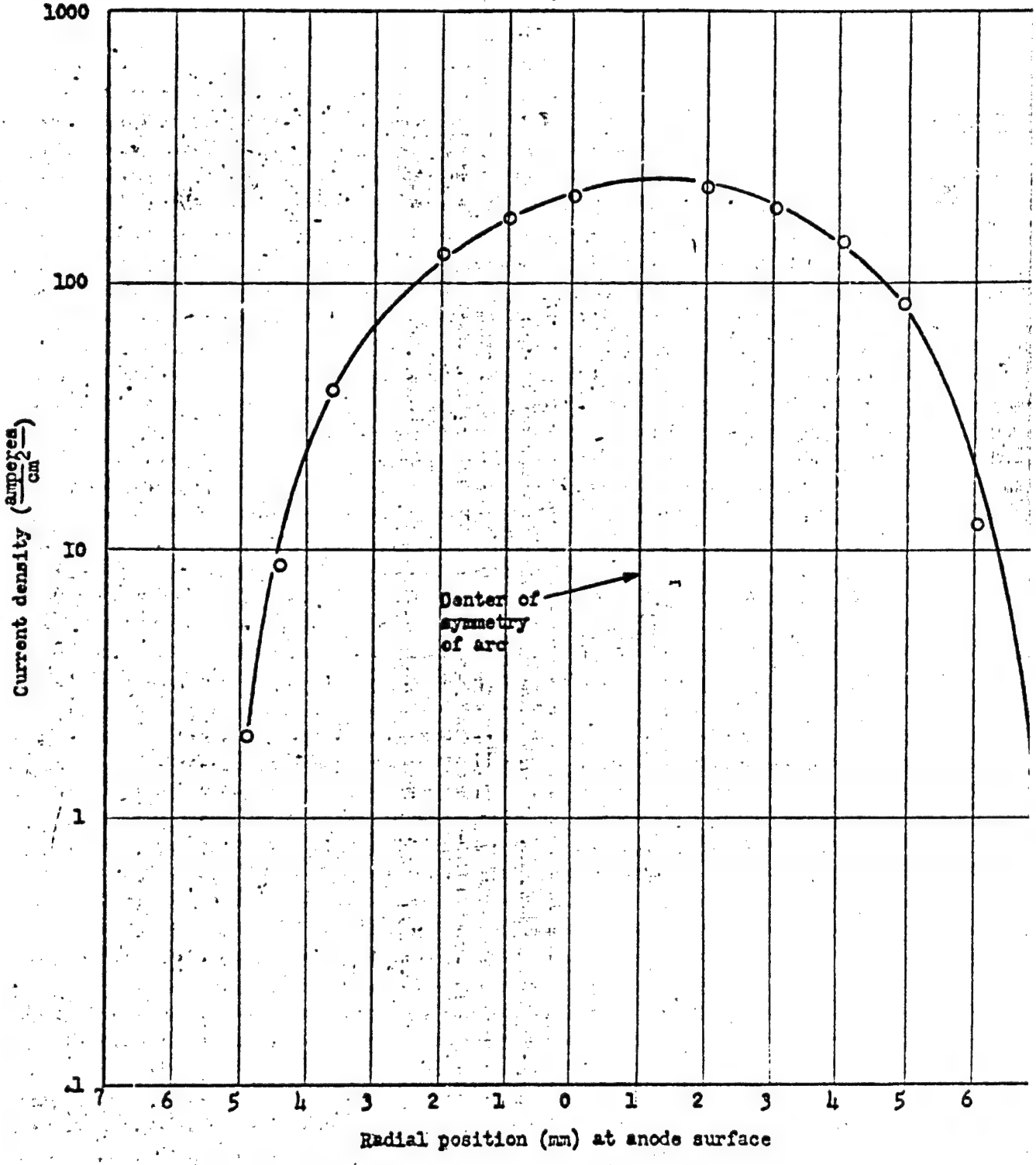

FIG. 22 CURRENT DENSITY vs ARC RADIUS IN HELIUM ARC at 230 AMPERES

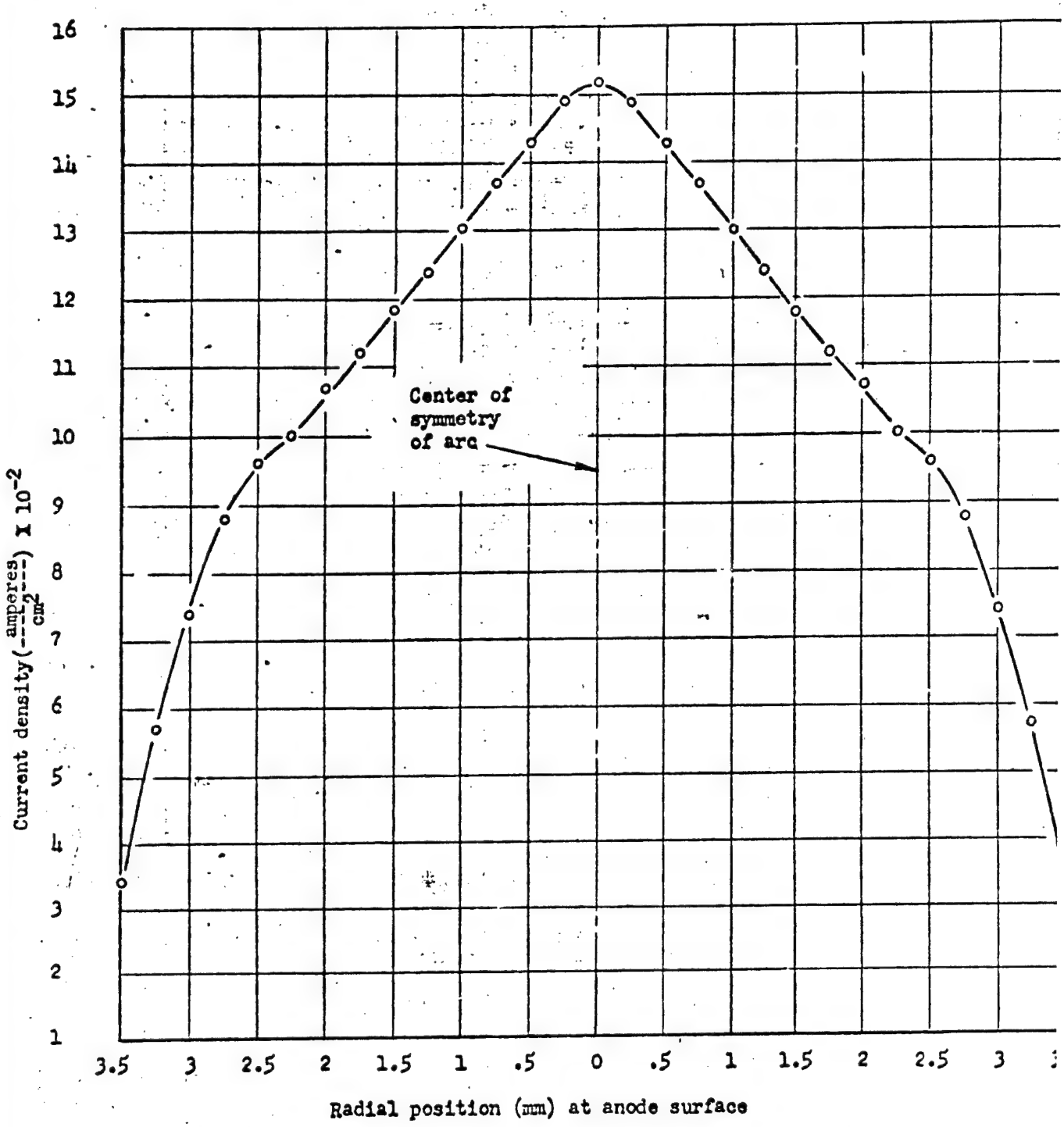

FIG. 23 CURRENT DENSITY vs ARC RADIUS IN AN ARGON -- NITROGEN ARC AT 350 AMPERES

(n_e, n_i, and n_a, respectively) as well as the ion-electron cross sections Q_e^i were all computed as functions of temperature for the gases of interest. The cross sections can therefore be computed as functions of temperature over a range which was determined spectroscopically for each particular gas. Even though the correction was small, the presence of doubly charged ions was included in the term ($n_i Q_e^i$) on the R. H. S. of Eq. (17).

Values obtained in this manner for cross sections in argon are shown in Figure 24. Making use of these values for argon and the known gas percentages in the argon-nitrogen arc, and writing the terms involving cross sections in Eq. (17) as sums over both argon and nitrogen contributions, cross sections for nitrogen can be obtained. These are given in Figure 25. Finally, for the case of helium, temperatures in the arc were measured only at positions which corresponded very nearly to 15,000°K. Therefore, the cross section was evaluated only at 15,000°K for helium and was found to be 2.09×10^{-15} cm^2.

At first sight, these cross sections seem somewhat larger than what may have been expected. However, recent theoretical work has raised estimates of these values by an order of magnitude or more for the temperature range under consideration here. For example, a straightforward use of the Born approximation for hydrogen yields a value of 3.5×10^{-16} cm^2 for the atom-electron collision cross section. Quantum mechanical calculations by Mower [26] and Massey and Morseiwitsch [27], on the other hand, increased this value to 25×10^{-16} cm^2. This latter value is in keeping with those obtained in our experiments.

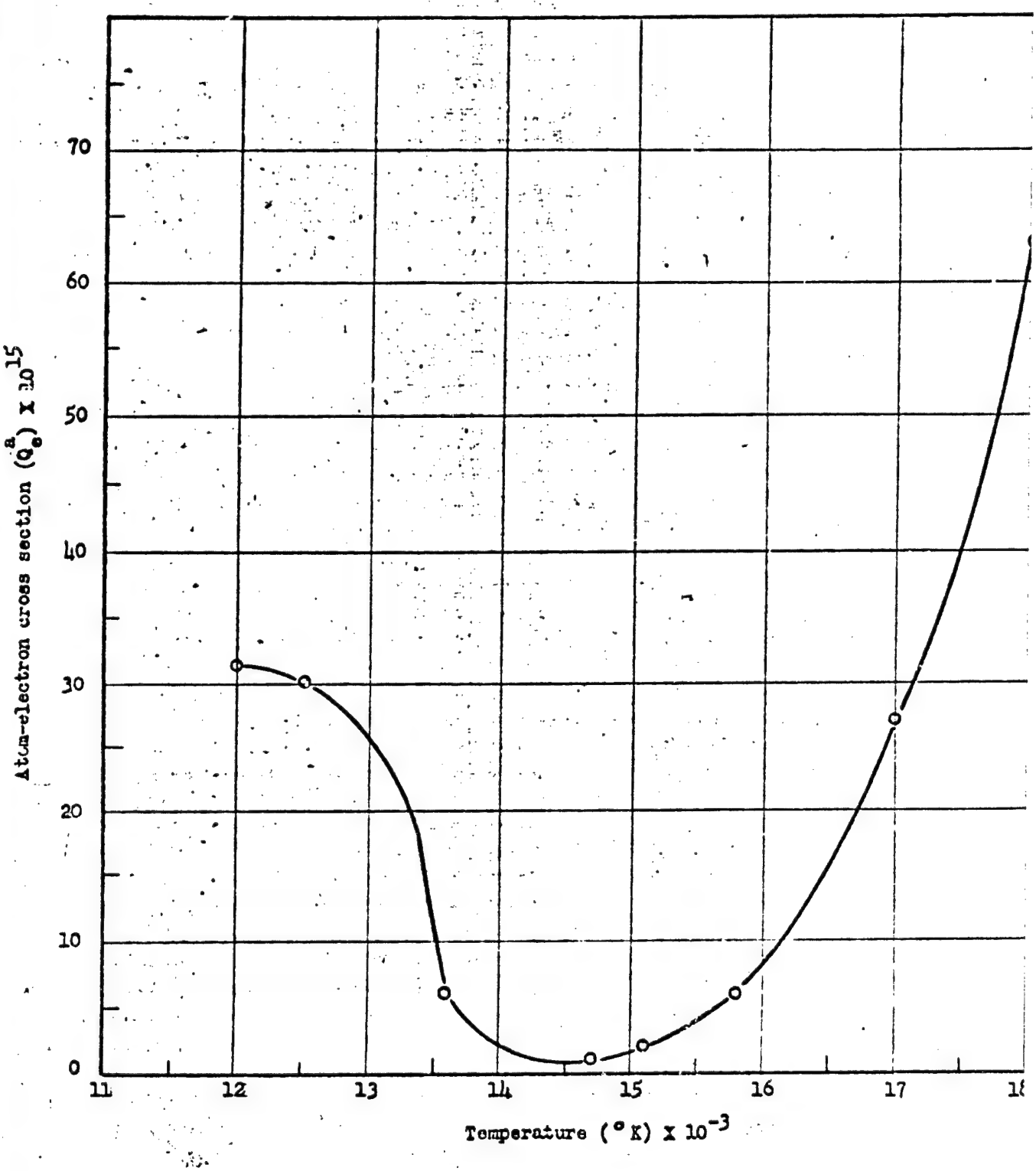

FIG. 24 ATOM-ELECTRON COLLISION CROSS-SECTIONS IN ARGON

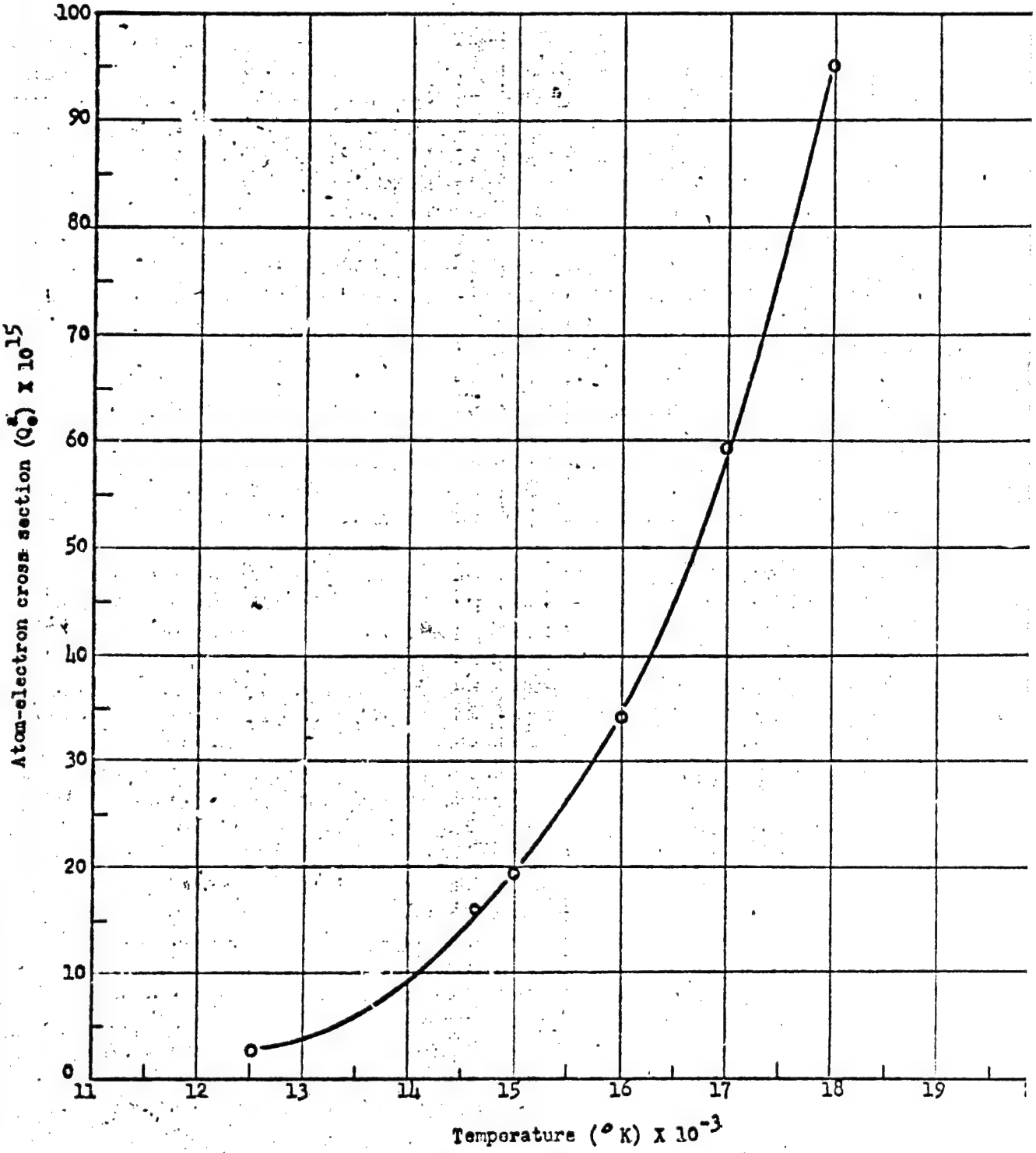

FIG. 2: ATOM-ELECTRON COLLISIONS CROSS SECTIONS IN NITROGEN

It should be mentioned here that results of previous work at higher energies have often been expressed in terms of a collision probability. This quantity is really the absorption coefficient divided by the gas pressure and is expressed in units of $(\text{cm} - \text{mm Hg})^{-1}$. Any such numbers can be converted to cross sections as given in this report upon multiplication by the numerical factor 2.81×10^{-17}.

3.2 TRANSPORT PROPERTIES

The measurable physical quantities in the arc columns (electric field, current density, temperature) were used to compute collision cross sections for argon, helium, and nitrogen. We shall now attempt to use the values for these cross sections in estimating certain transport properties for these gases.

To illustrate what must be done, we recall, for example, that the dynamical viscosity of a gas is given as

$$\eta = \frac{1}{3} n m \lambda \bar{v} \ . \qquad (18)$$

In this formula, $\bar{v}$ is the mean velocity of the atoms or molecules, λ is the mean free path, m is the mass, and n is the number density of the particles. Under normal conditions, the factor n can be eliminated using the relation $\lambda = 1/n Q$, where Q is the effective collision cross section. This shows that such properties as the viscosity are normally independent of pressure. However, with increasing temperature a certain portion of the gas becomes ionized. The properties of this partially ionized gas differ markedly from those of an

ordinary gas. There are now several collision cross sections which have to be considered: those for atoms against atoms, atoms against ions, and atoms against electrons. Equation (18) now becomes

$$\eta = \frac{1}{3} \Sigma_j n_j m_j \lambda_j \bar{v}_j \ , \tag{19}$$

where j refers to atoms, ions, and electrons. The mean free path for, say, the atoms in this situation is given as

$$\lambda_a = \frac{1}{n_a Q_a^a + n_i Q_i^a + n_e Q_e^a} \ . \tag{20}$$

It will be noted that now the factor n_i does not cancel, and a pressure-dependent form of η is obtained. This is essentially a result of the fact that in general the ionization equilibrium depends on the pressure.

Expanding Eq. (19), we obtain for the viscosity

$$\eta = \frac{n_a m_a \bar{v}_a}{3\left(n_a Q_a^a + n_i Q_i^a + n_e Q_e^a\right)} + \frac{n_i m_i \bar{v}_i}{3\left(n_i Q_i^i + n_a Q_i^a + n_e Q_e^i\right)} + \frac{n_e m_e \bar{v}_e}{3\left(n_e Q_e^e + n_i Q_i^e + n_a Q_a^e\right)} \ . \tag{21}$$

Here again, the subscripts a, e, and i refer to atoms, electrons, and ions, respectively. The last term in this equation can be neglected since the product $(m\,v)$ for electrons is small compared to that for the atoms or ions. In evaluating this equation, we take values for the

atom-atom cross sections from the literature [3, 28, 29] which have been estimated on the basis of kinetic theory. Further, we assume here that $Q_a^e \approx Q_a^i$. Values for the viscosity obtained in this manner for argon and nitrogen are given in Table 2 along with values previously calculated using theoretically estimated values for all of the cross sections. A value for η of 26.9×10^{-4} gm/cm-sec is computed for helium at 15,000°K on the basis of this work and can be compared with a value of 41.0×10^{-4} gm/cm-sec given in [29]. In general, the values obtained here are some 30 to 50 per cent lower than previously estimated and seem to be approaching a minimum near 2 ev, where the atom-electron collision cross sections are the highest.

The electrical conductivity, another transport property which was obtained by current density and electric field strength measurements, is shown for argon and nitrogen in Figures 26 and 27. A value of $\sigma = .65 \times 10^{13}$ esu was obtained for helium at 15,000°K. No direct comparison was made for this parameter with previous estimates. Considering the over-all experiment, it is felt that an accuracy of $\pm$ 15% may be attached to any of the figures given in this report. The largest single source of error may be expected to lie with the spectroscopic temperature measurements, which involve spectral plate calibration and other standard data reduction techniques.

Correlation of these properties and others is being continued for argon, helium, and nitrogen. Further, future experiments are expected to yield experimental data for hydrogen, krypton, and xenon, and this information will also be compared with data available in the literature.

Table 2. Viscosities for Argon and Nitrogen

$10^4 \eta$, g/cm-sec

Temperature °K	Argon		Nitrogen	
	Computed on Basis of Present Experiments	Ref. 29 Values	Computed on Basis of Present Experiments	Ref. 28 Values
10,000	20.1	31.0	----	21.2
12,000	18.5	35.5	19.4	22.6
14,000	17.3	39.8	14.3	19.5
16,000	16.0	----	3.8	----
18,000	14.8	----	0.90	----

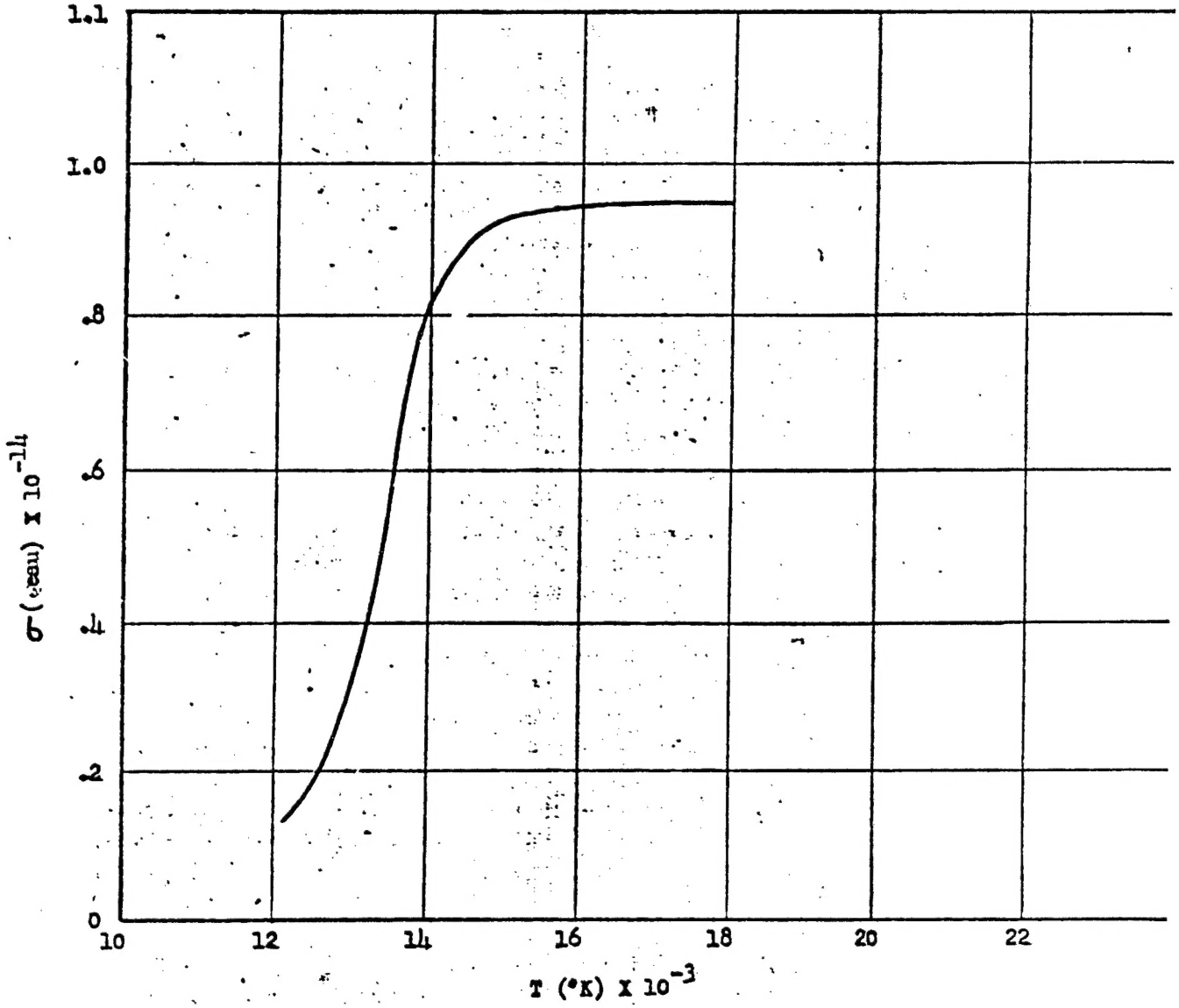

FIG. 26 ELECTRICAL CONDUCTIVITY vs TEMPERATURE FOR ARGON

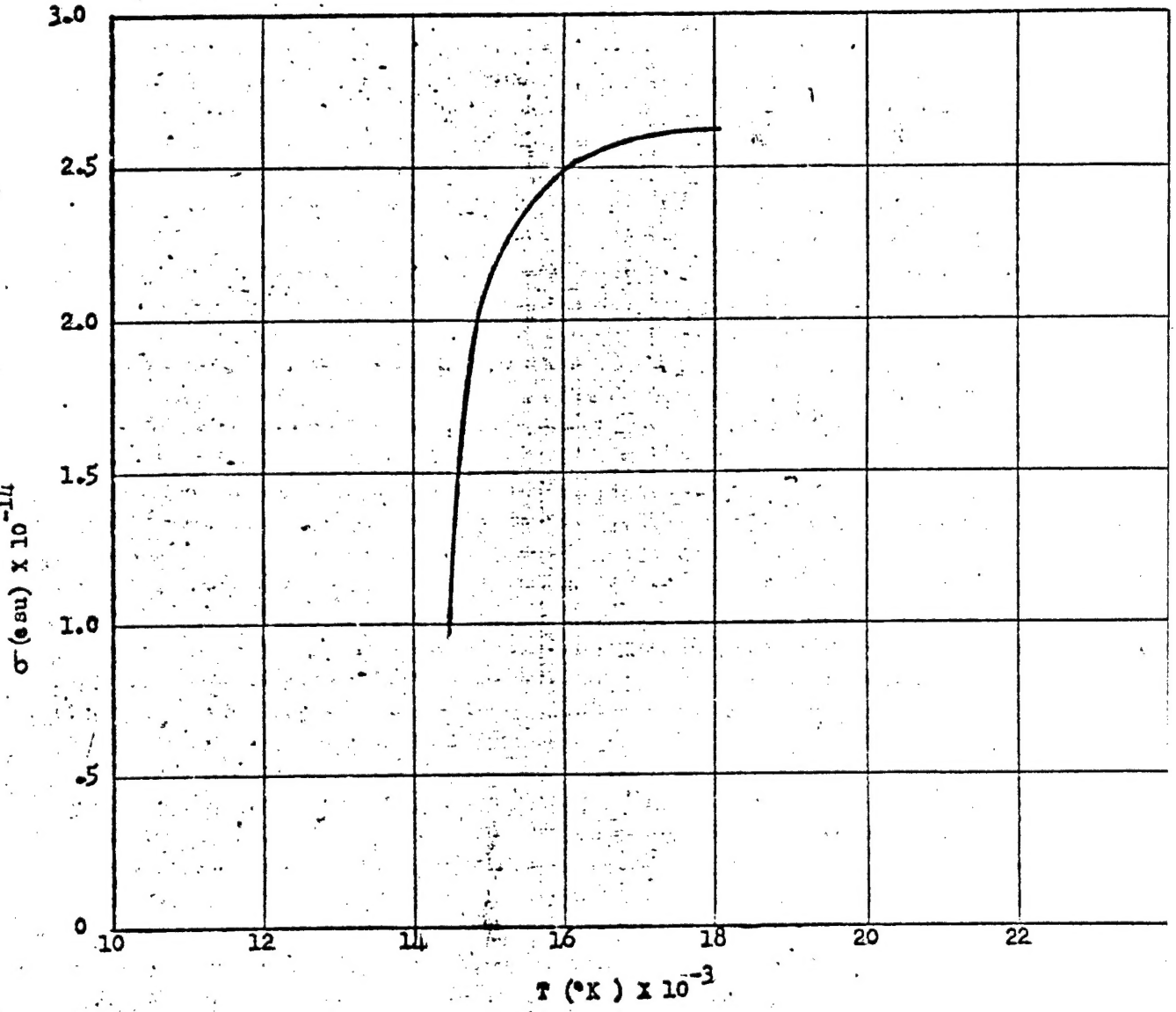

FIG. 27 ELECTRICAL CONDUCTIVITY vs TEMPERATURE FOR NITROGEN

4. BIBLIOGRAPHY

1. Griem, H. R., Plasma Spectroscopy, Proceedings of Fifth International Conference on Ionization Phenomena in Gases, Munich, 1961.

2. Finkelnberg, W., and Maecker, H., Handbuch der Physik, Vol. 22, (Springer Verlag Berlin) 1956.

3. Lochte-Holtgreven, W., Reports on Progress in Physics, 21, 312 (1958).

4. Lenard, P., Ann. der Physik, 12, 714 (1903).

5. Ramsauer, C., Ann. der Physik, 64, 513 (1921).

6. Mayer, H. F., Ann. der Physik, 64, 451 (1921).

7. Brown, S. C., Basic Data of Plasma Physics, John Wiley & Sons, 1959.

8. Olsen, H. N., Phys. Fluids, 2, 614 (1959).

9. Barr, T. A., and Cason, C., Quarterly Research Reviews, Army Rocket and Guided Missile Agency Report No. TN 1C1N-23, 1960.

10. Cason, C., and Smith, C. R., Quarterly Research Reviews, Army Rocket and Guided Missile Agency Report No. TN 1C1N-25, 1960.

11. Burhorn, F., and Wienicke, R., Zeitschr. für Physikalische chemie, 215, 269 (1960).

12. Spitzer, L., and Härm, R., Phys. Rev., 80, 230 (1950).

13. Spitzer, L., and Härm, R., Phys. Rev., 89, 977 (1953).

14. Gvosdover, S. D., Phys. Z. Sovjet, 12, 164 (1937).

15. Maecker, H., Peters, Th., and Schenk, H., Zeit. für Physik, 40, 119 (1955).

16. Optical Spectrometric Measurements of High Temperatures, Edited by P. J. Dickerman, University of Chicago Press, 1961.

17. Olsen, H. N., Private Communication.

18. Johnson, W. B., Private Communication.

19. Hattenberg, A. T., Dissertation, University of Maryland, 1961.

20. Richter, J., Zeits. für Astrophysik, 51, 177 (1961).

21. Nestor, O. H., S. I. A. M. Review, 2, 200 (1960).

22. Griem, H. R., Baranger, M., Kolb, A. C., and Oertel, G., Neutral Helium Lines (To be published).

23. Berg, H., Dissertation, University of Maryland, 1961.

24. Olsen, H. N., Proceedings of the 12th Gaseous Electronics Conference, NBS, 1959.

25. Gericke, W. E., Zeits. für Astrophysik, 53, 68 (1961).

26. Mower, L., Phys. Rev. 89, 947 (1953).

27. Massey, H. S. W., and Morseiwitsch, B. L., Proc. Roy. Soc., A205, 483 (1951).

28. Hansen, C. F., NACA Report TN 4150, 1958.

29. Amdur, I., and Mason, E. A., Phys. Fluids, 1, 370 (1958).